Theoretical advances in molecular bottlebrushes and comblike (co)polymers: solutions, gels, and self-assembly

Ekaterina B Zhulina, Sergei S Sheiko, Oleg V. Borisov

Soft Matter

REVIEW

Cite this: DOI: 10.1039/d2sm01141g

Theoretical advances in molecular bottlebrushes and comblike (co)polymers: solutions, gels, and self-assembly

Ekaterina B. Zhulina, *[a] Sergei S. Sheiko [ab] and Oleg V. Borisov *[ac]

Received 21st August 2022,
Accepted 19th October 2022

DOI: 10.1039/d2sm01141g

rsc.li/soft-matter-journal

We present an overview of state-of-the-art theory of (i) conformational properties of molecular bottlebrushes in solution, (ii) self-assembly of di- and triblock copolymers comprising comb-shaped and bottlebrush blocks in solutions and melts, and (iii) cross-linked and self-assembled gels with bottlebrush subchains. We demonstrate how theoretical models enable quantitative prediction and interpretation of experimental results and provide rational guidance for design of new materials with physical properties tunable by architecture of constituent bottlebrush blocks.

1 Introduction

Brush-like macromolecules remain a focus of extensive theoretical and experimental research for a few decades.[1–11] Intra- as well as intermolecular interactions between densely grafted side chains determine specific conformational and dynamic properties of brush macromolecules and materials thereof, as compared to conventional linear polymers.

A molecular brush consists of a linear chain backbone with multiple side chains tethered to it. There exist three synthetic approaches to fabricate molecular brushes: (i) ''grafting to'', when pre-synthesized side chains are covalently attached to a pre-synthesized main chain; (ii) ''grafting through'' polymerization of so-called macromonomers, and (iii) ''grafting from'', when polymerization of side chains is initiated from a properly functionalized backbone (macroinitiator). Each approach has pros and cons in terms of controlling backbone length, side chain dimensions, and grafting density. Additional structural complexity can be introduced through selective gradients in grafting density or block copolymers as side chains.[2,12,13]

The possibility to vary architectural parameters, such as side chain length and grafting density, in a wide range and independently from one another allows for controlling and adjusting static and dynamic properties of the solutions of graft polymers as well as mechanical properties of bulk materials and gels thereof.[2,6]

Furthermore, hierarchically branched architectures with structural bottlebrush motifs, such as barbwire[14–16] or dendronized polymers,[17,18] have been synthesized and their behavior has been explored and rationalized theoretically.[19–21] Combining branched architecture with temperature-, pH-, light-responsive functions in the main and side chains of the bottlebrushes opens fascinating new horizons for smart material design.[22–30]

Theory employing analytical[31–37] and self-consistent field numerical[38] approaches, as well as coarse-grained computer simulations[39–48] of comb-like, bottlebrush, and barbwire macromolecules and dendronized polymers, has been used to verify (corroborate) relationships between macromolecular architecture and experimentally accessible and technologically relevant properties of melts, solutions, and thin films.

Self-organization of block copolymers with chemically different incompatible comblike or bottlebrush blocks has recently attracted considerable attention because it can be exploited for fabrication of nanostructured materials, including physically crosslinked elastomers and mesogels with properties unattainable by using conventional linear block copolymers. It was demonstrated that microphase segregation in the melt of such bottlebrush block copolymers gives rise to materials with tissue-mimetic mechanical properties and structural colorations.[49–53] While theoretical principles of microphase segregation in the melt of linear–linear block copolymers are well-established,[54–58] and confirmed experimentally,[57,58] the understanding of the impact of brush architecture on microphase segregated morphology has been achieved only recently[59–69] and allowed explaining experimental data.[70–77]

Self-assembly of such block copolymers in selective solvents produces diverse nanostructures with dimensions and morphology controlled by the branched architecture of the blocks.[78–89] Moreover, structural properties of molecular aggregates may

[a] Institute of Macromolecular Compounds of the Russian Academy of Sciences, St. Petersburg, Russia
[b] Department of Chemistry, University of North Carolina at Chapel Hill, 27599, USA
[c] Institut des Sciences Analytiques et de Physico-Chimie pour l'Environnement et les Matériaux, UMR 5254 CNRS UPPA, Pau, France. E-mail: oleg.borisov@uiv-pau.fr

exhibit unusual dependences on the degrees of polymerization of the blocks that differ from those predicted and experimentally observed for micelles composed of linear block copolymers.[90,91]

Swelling of covalently crosslinked networks with brush-like strands in a good solvent leads to "haired gels".[92–96] Similar structures ("haired mesogels") arise upon self-assembly of triblock copolymers with a comblike or bottlebrush middle block and associating terminal blocks.[25,92] The swelling ratio and osmotic modulus of such gels depend in a complex way on grafting density and polymerization degree of the side chains decorating the network strands.[25,26,93]

The scope of this review is to present an overview of recent theoretical developments in increasingly complex polymer systems comprising comblike or bottlebrush building blocks and to compare theoretical predictions to experimental results.

The rest of the paper is organized as follows: in Section 2, we summarize theoretical results on conformations of molecular brushes in dilute and semi-dilute solutions, as well as in melts. In Section 3, we overview recent theoretical predictions of the swelling behavior and mechanical properties of haired gels with brush-like subchains. Self-assembly of these block copolymers in selective solvents and the formation of colloidal nanostructures is described in Section 4. Microphase segregation in melts of block copolymers comprising chemically different brush blocks is described in Section 5 with particular emphasis on comparison between theoretical predictions and experimental data. In Section 6, we formulate conclusions and outline perspectives for further development in theory and modelling of bottlebrush architectures and the potential of applications of materials based on comblike and bottlebrush (co)copolymers.

2 Solutions of bottlebrushes

2.1 Molecular brushes *versus* comblike polymers

A comblike or a bottlebrush macromolecule consists of a long main chain ("backbone") with multiple side chains ("grafts") covalently attached to it. When more than one side chain emanate from each branching point the macromolecule is termed "barbwire". In the majority of reported systems, side chains are linear polymers. However, the grafts may exhibit more complex topology, *e.g.* dendritic (in so-called dendronized polymers[17,18]) or even comblike.

The utilization of terms "comblike" or "bottlebrush" macromolecule is sometimes confusing. We apply terms bottlebrush (bb) and comblike (cl) to macromolecules with the backbone conformation perturbed or non-perturbed by interactions between side chains, respectively. Note that the application of this criterion to different systems (architectures, solutions, and melts) may produce different boundaries between the comb and brush regimes in terms of specific architectural parameters.

Below we focus on the most generic class of brush macromolecules comprising the main chain with a degree of polymerization (DP) $M \gg 1$ and linear side chains with DP n tethered to every m-th monomer unit of the backbone, Fig. 1. The overall DP of such macromolecule is

$$N = M(1 + n/m) \quad (1)$$

The number of grafts $P = M/m \gg 1$. For quantitative mapping of this theoretical model to a real experimental system, one has to account for possible differences in volumes of monomer units in main and side chains, as well as their solubility and flexibility or bending rigidity. In our discussion, we disregard

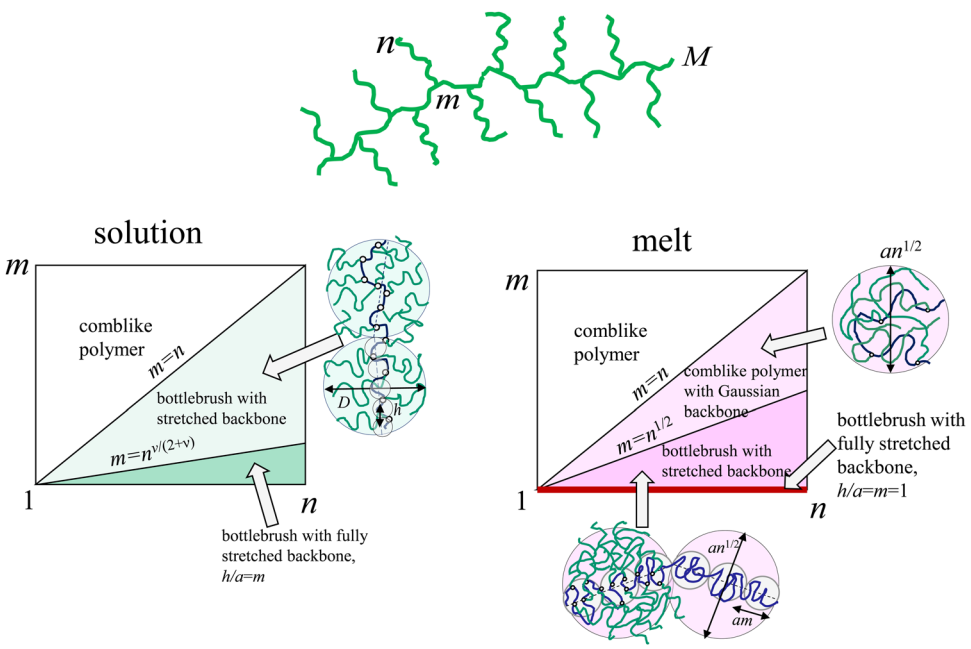

Fig. 1 Diagrams of state for comblike polymers and bottlebrushes in solution and in the melt. The set of architectural parameters: M is the DP of the main chain, n is the DP of a side chain, m is the number of monomer units in the segment of the main chain separating neighbouring grafting points (a spacer).

these differences and focus only on the effect of architecture {*M*,*n*,*m*} on large scale conformational and thermodynamic properties of the bottlebrushes in solutions and melts. Therefore, we assume statistical segments in both main and side chains to have approximately equal length $\sim a$ and volume $\sim a^3$.

In dilute solution (under good or theta-solvent conditions), the repulsive interactions between the grafts provoke extension of both the grafts and separating them spacers with respect to their unperturbed dimensions when neighboring grafts start to overlap, that is at $m \simeq n$. In melt, the extension of the backbone with respect to the Gaussian dimensions occurs only at much shorter spacer length, $m \sim n^{1/2}$.[97–99] At $m \geq n^{1/2}$ the backbone exhibits the Gaussian statistics on all length scales, whereas side chains retain in the melt the Gaussian size at any spacer length $m \gtrsim 1$. Hence, a macromolecule with the DP of spacers $n^{1/2} \leq m \leq n$ behaves as a molecular brush in solution, but as a comblike polymer in melt. The quantitative criteria for discrimination between comblike and bottlebrush polymers should be modified for more complex architectures of the grafts, *e.g.*, for ''barbwire'' or dendronized polymers.

2.2 Conformations of molecular brushes in dilute solution

Conformational and elastic properties of bottlebrushes in dilute and semi-dilute solutions were rationalized on the basis of the scaling approach,[31–35] complemented by numerical self-consistent field (SCF) theory,[38] and the theoretical findings were confirmed by experiments and computer simulations.[39–47]

Local and large-scale conformational properties of molecular brushes in solutions are determined by strong repulsive interactions between adjacent side chains under conditions of their strong overlap. Repulsions between side chains in a good or theta-solvent are due to binary or ternary repulsive interactions acting between monomer units, respectively. These repulsions lead to stretching of the side chains in the radial direction and cause axial (tensile) stress in the main chain. If the main chain is flexible, *i.e.*, each spacer separating neighboring grafts includes at least a few statistical segments, then the main chain also becomes stretched on a scale larger than or comparable to the thickness of the bottlebrush controlled by the radial extension of the side chains. As a consequence, the molecular brush acquires a local cylindrical symmetry on a scale comparable or greater than the characteristic size of the elongated side chains.

Theory[31,34] provides scaling relations between molecular parameters {*m*,*n*} and dimensions of side chains (the brush thickness *D*), and end-to-end distance *h* of spacers in the form

$$D/a \cong \begin{cases} n^{\nu}(n/m)^{\nu(1-\nu)/2}, & m \geq m^* \\ n^{2\nu/(1+\nu)}m^{-(1-\nu)/(1+\nu)}, & m \leq m^* \end{cases} \quad (2)$$

$$h/a \cong \begin{cases} m^{\nu}(n/m)^{\nu(1-\nu)/2}, & m \geq m^* \\ m, & m \leq m^*, \end{cases} \quad (3)$$

where $m^* \cong n^{\nu/(2+\nu)}$ and ν is the Flory exponent equal to ≈ 0.6 or 0.5 under good or theta-solvent conditions, respectively. The first and the second lines in eqn (2) and (3) correspond to partial and limiting (up to the contour length, *m*) stretching of spacers of the main chain, respectively. As follows from eqn (2) and (3), under conditions of overlap of side chains, $n/m \gg 1$, spacers and side chains get stretched with respect to their unperturbed dimensions, m^{ν}/a and n^{ν}/a, under both good and theta-solvent conditions due to binary or ternary repulsions between monomer units, respectively. At this point it is convenient, following ref. 31, to introduce the concept of a ''superblob'' as a symmetric segment of the molecular brush of size equal (with the accuracy of a numerical factor) to *D*. Because of repulsive interactions and stretching of the side chains, the superblobs are virtually impermeable, that is, their overlap would lead to the free energy penalty exceeding k_BT. Notably, the same scaling relation holds between the size *D* and number of side chains in the superblob, *D*/*h*, as for a starlike polymer[100,101] with *D*/*h* arms, *i.e.*, $D \cong n^{\nu}(D/h)^{(1-\nu)/2}/a$. We remark that the power law dependences (scaling relations) given by eqn (2) and (3) have asymptotic character, that is, apply only for $n, m \gg 1$. In real experimental and simulation systems usually $n \leq 10^2$ and $m \sim 1$. Because of cylindrical symmetry, a strong overlap of moderately long side chains is ensured only close to the backbone and, therefore, as demonstrated by numerical modelling, the predicted by eqn (2) and (3) scaling dependences on *n* are usually hardly reached.

Eqn (2) and (3) were derived in ref. 100, based on the representation of a cylindrical brush of side chains with axial distance *h* per chain as an array of concentric shells of densely packed concentration blobs of size $\xi(\rho) \cong (\rho h)^{1/2}$, where ρ is radial distance from the main chain, and, therefore, the volume fraction of monomer units of the side chains[102]

$$c(\rho) \cong (\xi/a)^{-(3\nu-1)/\nu} \cong (\rho h/a^2)^{-(3\nu-1)/2\nu} \quad (4)$$

Then the thickness $D/a \cong n^{2\nu/(1+\nu)}(h/a)^{-(1-\nu)/(1+\nu)}$ follows from the condition of conservation of the number of monomer units in the side chain

$$h\int_0^D c(\rho)\rho \mathrm{d}\rho = na^3 \quad (5)$$

As long as the spacers of the main chain do not reach the limit of their extensibility, *i.e.*, $h \leq m/a$, the equilibrium extension *h* of the spacers is found from the balance of the elastic free energy of the extended spacer[102]

$$\frac{F_{\mathrm{elastic}}}{k_BT} \cong \frac{h^{1/(1-\nu)/a}}{m^{\nu/(1-\nu)}} \quad (6)$$

and the free energy of the brush evaluated (in k_BT units) as a number of concentration blobs per side chain

$$\frac{F_{\mathrm{conc}}}{k_BT} \cong h\int_0^D \frac{\rho \mathrm{d}\rho}{\xi^3(\rho)} \cong (D/h)^{1/2} \quad (7)$$

To describe large-scale conformational properties of molecular brushes in solutions, a coarse-grained model assimilating the molecular brush to an equivalent wormlike chain with an effective thickness *D*, determined by the dimensions of the

extended side chains and the effective contour length

$$L \cong \frac{M}{m}h, \tag{8}$$

where h is the end-to-end distance of an extended spacer, is applied. The effective contour length, L, is, in the general case, smaller than the contour length of the fully elongated main chain because of local bending fluctuations of the main chain on a length scale smaller than D. Bending fluctuations of a molecular brush on the scale larger than D are controlled by an effective (or apparent) persistent length l_p. This length comprises contributions of the "intrinsic" rigidity (persistent length) of the main chain and "induced" rigidity due to enhanced repulsive interactions of side chains upon bending of the molecular brush.

Long, $L \gg l_p$, molecular brushes behave under conditions of both good and theta solvent for the main and side chains like self-avoiding wormlike chains, Fig. 2. This is because even under theta-solvent conditions, the ternary repulsive interactions of densely grafted side chains lead to a significant increase in the free energy upon overlap of the remote along the main chain segments of the molecular brush, thus creating an effectively excluded volume $\sim D^3$ of the molecular brush segment with the length equal to its thickness D.

The problem of flexibility of bottlebrushes in solution remained a subject of controversial discussions in the literature[10,31,32,38,46,47] because of systematic disagreement between the theoretical prediction in ref. 32 and the results of real and computer experiments. The controversy was resolved on the basis of self-consistent field modelling[38] supported by the results of extensive computer simulations.[46,47] It was demonstrated that due to azimuthal repartition of side chains upon bending of the molecular brush, the induced persistence length, $l_p \gg D$, is manifested only in dense molecular brushes with the DP of side chains $\geq 10^2$ and the approach to the predicted[32] dependence $l_p \sim D^2$ occurs only at extremely long side chains. Bending rigidity of molecular brushes with shorter (experimentally relevant) side chains is controlled by the brush thickness, $l_p \cong D$.

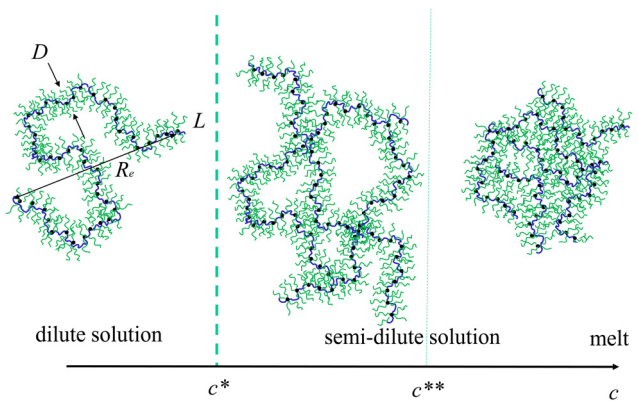

Fig. 2 Scaling regimes of dilute and semi-dilute solutions of molecular brushes. Threshold concentrations c^* and c^{**} correspond to the overlap of individual molecular brushes and to close packing of the constituent superblobs, respectively.

Hence, on length scales smaller than D, side chains form a cylindrical brush around the stretched backbone, while on length scales larger than D, the molecular brush behaves as a flexible self-avoiding chain composed of L/D impermeable subunits ("superblobs") each of size D, that is, the overall size of the molecular brushes in dilute solution scales as

$$R_{eq} \cong L^{\nu}D^{1-\nu} = \left(\frac{M}{m}\right)^{\nu} h^{\nu}D^{1-\nu} \tag{9}$$

In eqn (9), $\nu \approx 0.6$ is the Flory exponent in a good solvent. We remind that within the accuracy of scaling approximation, all the numerical prefactors on the order of unity are ignored and, therefore, eqn (9) corresponds (with the accuracy of omitted numerical coefficients) to any characteristic dimensions of the bottlebrush, *e.g.* radius of gyration or hydrodynamic radius or end-to-end distance of the main chain. With account of eqn (2) and (3)

$$R_{eq}/a \cong \begin{cases} N^{\nu}(n/m)^{\nu(1-3\nu)/2}, & m \geq m^* \\ N^{\nu}(n^{\nu}/m)^{(1-3\nu)/(1+\nu)}, & m \leq m^* \end{cases} \tag{10}$$

or

$$R_{eq}/a \cong \begin{cases} M^{\nu}(n/m)^{3\nu(1-\nu)/2}, & m \geq m^* \\ M^{\nu}n^{2\nu(1-\nu)/(1+\nu)}m^{-(1-\nu)^2/(1+\nu)}, & m \leq m^* \end{cases} \tag{11}$$

Eqn (10) and (11) illustrate that characteristic dimensions (*e.g.* end-to-end distance, gyration or hydrodynamic radius) of the molecular brush in dilute solution are systematically smaller than dimensions $\sim N^{\nu}/a$ of the linear chain with the same total DP N, but larger than dimensions $\sim M^{\nu}/a$ of a "bare" backbone due to intramolecular repulsions of densely grafted side chains.

2.3 Conformations of molecular brushes in semi-dilute solutions and extensional elasticity

Scaling theory of semi-dilute solutions of molecular brushes was developed in ref. 33 and 34. The solutions of long (comprising multiple superblobs, $L \gg D$) molecular brushes exhibit hierarchical structural organization through multiple length scales: on the large scale the bottlebrush behaves as a flexible wormlike macromolecule, whereas on the length scale smaller than the brush thickness D it exhibits the structure of a cylindrical polymer brush. Due to the presence in the system of several characteristic length scales (local correlation length or the concentration blob size ξ, the molecular brush thickness D and its total radius of gyration R_{eq}) one can distinguish several characteristic (threshold) values of the polymer solution concentration and formulate the associated scaling laws for the structural and thermodynamic properties for solutions of molecular brushes.

A progressive increase in the solution concentration and crossing over a sequence of thresholds results in screening of excluded volume interactions and structural re-arrangement in the solution of bottlebrushes on progressively decreasing length scales.

Local conformational properties of the molecular brushes in dilute solution are characterized by stretching of both side chains and spacers. This local conformational structure is preserved in the regime of semi-dilute solution at concentrations $c^* \leq c \leq c^{**}$, where c^* is average intramolecular concentration (volume fraction) in the volume occupied by the molecular brush in the dilute solution,

$$c^* \cong \frac{M(1+n/m)a^3}{R_{eq}{}^3}, \quad (12)$$

(which is equal to the overlap concentration directly related to intrinsic viscosity $[\eta]$ as $[\eta]c^* \sim 1$) whereas

$$c^{**} \cong \frac{na^3}{hD^2} \quad (13)$$

is average concentration of the monomer units inside the superblobs. The larger the DP M of the main chain the smaller the first overlap concentration c^* and the wider the regime $c^* \leq c \leq c^{**}$ because c^{**} is independent of M (see eqn (13)). The overall dimensions of the molecular brush decrease in this regime as a function of the solution concentration c due to screening of intramolecular repulsions on the length scales larger than D and follow scaling dependence $R_{eq}(c) \sim ac^{-(2\nu-1)/2(3\nu-1)}$ typical for semi-dilute solutions of linear chains in a good solvent.

Above c^{**} which corresponds to close packing of the superblobs, screening of excluded volume interactions between side chains becomes efficient on the length scale smaller than the brush thickness D. As a result, both side chains and spacers reduce their extension and the size of the bottlebrush as a whole further decreases. If in dilute solution spacers were fully extended, that is the case at $m \leq m^*$, this full extension is relaxed at $c \geq c^{(m)} \cong m^{-2(3\nu-1)/\nu}$. Remarkably, on the length scale $\sim D$ close-packed superblobs remain mutually impermeable (segregated) because of residual stretching of the side chains.

Eventually, at concentrations $c \geq c^{***} \cong m^{-(3\nu-1)}$ spacers and side chains lose their stretching and acquire conformations of Gaussian chains of the concentration blobs with size $\xi \cong ac^{-\nu/(3\nu-1)}$. Subsequent increase in concentration c towards the melt state leads to shrinkage of the main and side chains and a decrease in the overall dimensions of the molecular brush. Different regimes of dilute and semi-dilute solutions of molecular brushes are schematically depicted in Fig. 2.

Conformations of molecular brushes in the melt, *i.e.*, at $c \cong 1$ were analyzed in ref. 99. It was demonstrated, that at $n^{1/2} \leq m \leq n$ both side chains and the backbone in the melt have conformations of Gaussian coils. However, for dense brushes with $m \leq n^{1/2}$ the space filling constraints impose partial stretching of the backbone on the length scale on the order of the Gaussian size of the side chain, $\sim an^{1/2}$.

The extensional deformation of an individual molecular brush leads to intramolecular structural re-arrangement on a progressively decreasing length scale.[34] As a result, the force *versus* deformation curves exhibit more complex patterns than those for linear chain molecules both in dilute and in semi-dilute solutions.

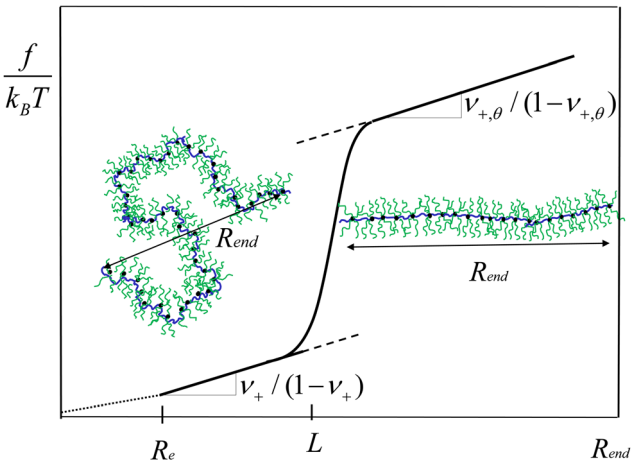

Fig. 3 Restoring elastic force, *f*, *versus* end-to-end distance, R_{end}, of the main chain of a stretched molecular brush (in double log coordinates). Linear response regime is indicated by dotted line. Here $\nu_+ \cong 0.6$ and $\nu_\theta = 1/2$ are the Flory exponents under conditions of good and theta-solvents for the monomer units of the main chain, respectively.

The force–extension curves, that is the dependence of the restoring elastic force f on the end-to-end distance R_{end} for molecular brushes with long main chain exhibit a sigmoidal shape (Fig. 3): a linear response regime at $R_{end} \geq R_{eq}$ is followed by a non-linear one characteristic for the self-avoiding chain power law $f \sim R_{end}{}^{\nu/(1-\nu)}$ at relatively weak deformation ($R_{eq} \leq R_{end} \ll L$); the conformations of side chains and spacers are not affected by deformation, but repulsive interactions between the side chains make the molecular brush softer than the "bare" backbone. A sharp hardening occurs at intermediate extension ($R_{end} \cong L$) when the molecular brush is assimilated to the fully stretched chain of superblobs and further extension requires that the backbone spacers get additionally stretched by external force which exceeds the equilibrium axial tension in the backbone of a "free" (non-stretched) bottlebrush. The elastic response of a "bare" backbone is eventually recovered at stronger deformation, $L \leq R_{end}$. Computer MC simulations on the end-stretched bb polymers[103,104] indicated two regimes for $f(R_{end})$ behavior: linear response $f \sim R_{end}$ for all side chain lengths (including linear chains, $n = 0$), followed by the non-linear elasticity regime. Although the backbone in the simulated polymers was long enough ($M \simeq 10^3$), the side chains were relatively short ($n \leq 20$) which could compromise swelling and impermeability of the superblobs presumed in the scaling model.

An increase in the solution concentration c results in screening of intramolecular repulsions on progressively decreasing length scales, which diminishes the "softening" effect and leads to stronger elastic response of the molecular brush to extensional deformation in semi-dilute solution than in the dilute solution. The described above sigmoidal shape of the force–extension curve is typical only for brushes with sufficiently long spacers that exhibit pronounced flexibility in the unperturbed state. In contrast, in the brush with dense grafting of side chains, $m \leq m^*$, repulsions of side chains assure softening of the brush in the whole range of deformations except for limiting extension.

2.4 Molecular brushes in poor solvent

Coil-to-globule transition in an individual molecular brush in a poor solvent was analyzed in ref. 35 and 90. Under theta-solvent conditions, volume fraction $c(\rho)$ of monomer units at distance ρ from the backbone of the bottlebrush can be obtained from eqn (4) by implementing $\nu = 1/2$ that leads to

$$c(\rho) \simeq \left(\frac{a^2}{h\rho}\right)^{1/2} \tag{14}$$

and thickness D of the bottlebrush (superblob size) yields

$$D/a \simeq n^{2/3}(h/a)^{-1/3} \tag{15}$$

with the last concentration blob $\xi(\rho = D) \simeq ac(D)^{-1} \simeq (hD)^{1/2} \ll D$.

Inferior solvent strength, *i.e.*, an increase in $\tau = (\theta - T)/T$, leads to collapse of cylindrical brushes inside superblobs. The onset of the collapse is specified by the equality in sizes of the outermost concentration blob, $\xi(D) \simeq (Dh)^{1/2}$, and the thermal blob, $\xi_t(\tau) \simeq a/\tau$, to specify the transition point

$$\tau = \tau^* \simeq n^{-1/3}(h/a)^{-1/3}, \tag{16}$$

where h is given by eqn (3) with $\nu = 1/2$.

Therefore at $\tau \geq \tau^*$ the average volume fraction of monomer units in the superblobs is the same as in the collapsed polymer globule, that is, $c \simeq \tau$. In the vicinity of $\tau \cong \tau^*$, the second virial coefficient υ_D of superblob interactions changes from $\simeq D^3$ to $\simeq -D^3$ which causes collapse (coil-to-globule transition) of the molecular brush as a whole with the average end-to-end distance $R_{end} \simeq a(N/\tau)^{1/3}$.

3 Haired polymer gels

Swelling of covalent networks with brush-like strands in a good solvent yields the so-called "haired" gels. In contrast to gels with linear chain strands, the swelling and elastic properties of haired gels depend not only on the cross-linking density defined by the total DP N of a network strand, but also on the DPs and grafting density of side chains $\{n,m\}$ at a given backbone DP M. For the same crosslink density (the same N), variation of the architectural triplet $\{M,n,m\}$ results in different network topologies and correspondingly different swelling and mechanical properties. The equilibrium swelling ratio of such networks is shown to be larger than that of conventional linear chain networks as a result of two effects: architectural disentanglement of network strands and amplification of polymer–solvent interactions by side chains (higher number of monomers per backbone unit length).[26,93]

The equilibrium properties of haired gels can be described[95,96] using the same scaling principles as described above for semi-dilute solutions of molecular brushes. The equilibrium concentration of monomer units in a free-swelling gel (and thus the degree of swelling) in contact with the reservoir of solvent cannot be arbitrarily set but results from a balance of osmotic pressure inside the gel and elasticity of the strands.

Because of the topological constraints caused by densely grafted side chains, distribution of polymer density within the gel is, in the general case, inhomogeneous. Depending on the ratio between the gel mesh size (*e.g.* the end-to-end distance R_{end} of the main chains of the strands) and the side chain dimensions (the superblob size D) two structural regimes – hollow mesh and filled mesh – can be distinguished.[95,96] In the hollow mesh regime each strand constitutes a bottlebrush with thickness D, and the neighboring strands do not overlap producing hollow space (mesh) in between. In this case, the equilibrium swelling of the gel (the mesh size) can be evaluated directly using the c^*-theorem of de Gennes to give $R_{end} \simeq R_{eq}$. In the filled mesh regime, bb strands overlap and superblobs are perturbed. The interior of the gel can be assimilated to a quasi-uniform close-packed array of the concentration blobs with size $\xi(c) \sim ac^{-\nu/(3\nu-1)} < D$. In this case, the equilibrium swelling results from the balance of osmotic pressure $\pi/k_BT \cong \xi^{-3}(c)$ with the conformational elasticity of the main chains that is renormalized according to polymer concentration c inside the gel. Schematics in Fig. 4 illustrate the equilibrium gel structure with hollow (a) and filled (b) mesh.

As demonstrated in ref. 95, an increase in DP and/or grafting density of the side chains results in the monotonous increase in the gel volume V. In scaling terms, the mesh size $\simeq V^{1/3}$ follows eqn (10). However, the swelling ratio with respect to the dry gel volume, $V/V_{dry} \simeq {R_{eq}}^3/Na^3$, exhibits non-monotonous behavior and passes through a maximum as a function of DP n of the side chains when spacers in the strands reach the limit of their extensibility, that is at $n \cong m^{(\nu+2)/\nu}$.

In Fig. 5 the predicted[96] scaling dependence for the equilibrium swelling ratio, $V/V_{dry} \simeq M^{3\nu-1}(n/m)^{(3\nu-1)(2-3\nu)/2}$, is checked for chemically cross-linked gels with $m \simeq 1$ and fixed DP n of the side chains in bb strands.[93] The strands are constituted of polymerized macromonomers (MM) with norbornene backbone and poly(*n*-butyl acrylate) side chains and cross-linkers (XL). Variations in the system composition, [MM]/[XL], were linked to the average backbone length M of polymerizing bb strands as [MM]/[XL] $\sim M$. The equilibrium swelling ratio (V/V_{dry}) of these networks in toluene (indicated by symbols) is presented in Fig. 5 as a function of ratio [MM]/[XL]. Although toluene is thermodynamically a good solvent for

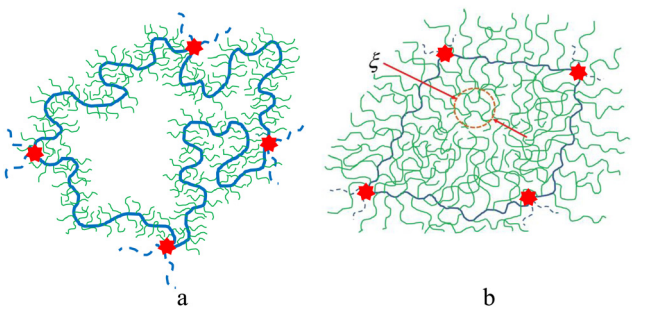

Fig. 4 Schematic of the gel with bottlebrush strands with hollow mesh (a) and filled mesh (b). Concentration correlation volume with length ξ is indicated by the red dashed circle.

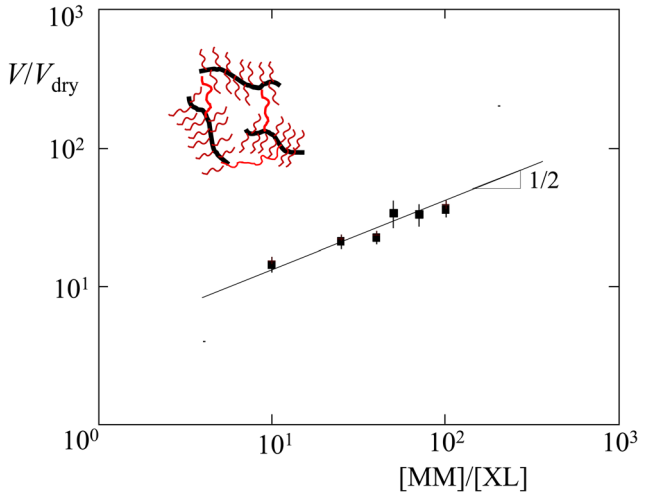

Fig. 5 Equilibrium swelling ratio V/V_{dry} *versus* macromonomer [MM] to cross-linker [XL] ratio in chemically cross-linked gel with bottlebrush strands (norbornene backbone and *n*-butyl acrylate side chains and cross-linkers in toluene). Data from Table 1 in ref. 93. Linking the system composition to the average length M of bb strands as [MM]/[XL] M, the slope in $V/V_{dry}\ M^{(3\nu-1)}$ dependence is indicated by the solid line for $\nu = 1/2$. Schematic in inset shows the gel bb backbones in black and side chains and cross-linkers in red.

PnBA, relatively short side chains (as well as longer cross-linkers) are still far from the scaling limit with $\nu = 3/5$, and the slope of the theoretically predicted dependence $V/V_{dry} \sim M^{3\nu-1}$ with exponent $\nu = 1/2$ (*i.e.*, the Gaussian statistics for a chain end-to-end distance) is in accord with the experimental data.

In Fig. 6 the normalized swelling ratio $(V/V_{dry})M^{-1/2}$ of chemically cross-linked poly(*n*-butyl acrylate) gels with varied architectures of bb strands[94] is presented as a function of the strand composition (n/m). Although the data in Fig. 6 is rather scattered, the trends are consistent with the scaling model[96]

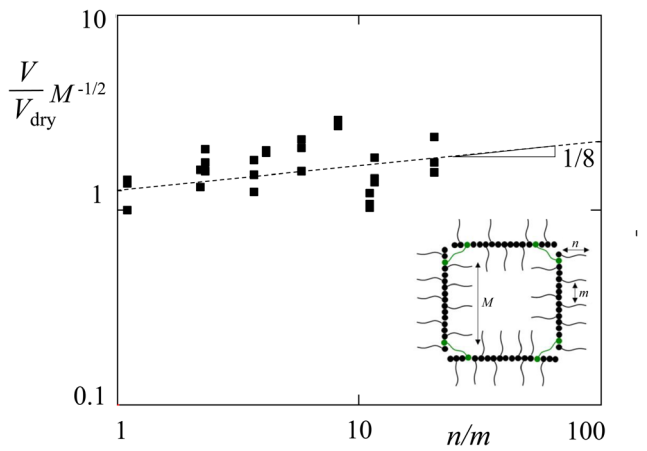

Fig. 6 Normalized experimental swelling ratio V/V_{dry} *versus* n/m in chemically cross-linked *n*-butyl acrylate gels with varied lengths of side chains (n) and spacers (m) in bb strands. Experimental data (Table in ESI in Sheiko *et al.*[94]) are normalized according to scaling prediction $(V/V_{dry})M^{1-3\nu} \sim (n/m)^{(3\nu-1)(2-3\nu)/2}$ with $\nu = 1/2$ to give $(V/V_{dry})M^{-1/2} \sim (n/m)^{1/8}$ with the numerical prefactor on the order of unity. Slope 1/8 is indicated by the dashed line.

predicting a weak increase in the normalized swelling ratio as a function of the strand composition, $(V/V_{dry})M^{-1/2} \sim (n/m)^{1/8}$, with the numerical prefactor on the order of unity.

An even more peculiar feature of the haired gels predicted by the scaling theory[96] is non-monotonous dependence of the bulk osmotic modulus G on DP n of the side chains: in the hollow mesh regime the bulk osmotic modulus is proportional to the inverse mesh volume, $G/k_BT \sim R_{eq}^{-3}$, and decreases as a function of n (see eqn (10)). However, in the filled mesh regime the modulus is controlled by the correlation length (concentration blob size) as $G/k_BT \sim \xi^{-3}(c)$ and, therefore, increases as a function of n. Hence, the scaling theory predicts a minimum in the bulk osmotic modulus of the haired gel as a function of n at the crossover from the hollow to the filled mesh regimes.

4 Micelles of bottlebrush block copolymers

Self-assembling copolymers with various architectures remains the focus of intensive research (see, *e.g.* reviews[105–107]) due to emerging applications in drug delivery,[108] biomimetic materials design,[109] tissue-engineering,[52] *etc.* The most investigated AB diblock copolymers associate in micellar structures (spherical, wormlike, vesicles) in a selective solvent, which is good for one block and poor for another. Spherical micelles are conventionally classified as crew-cut (with the corona thickness smaller than the core size) and starlike (with the corona thickness larger than the core size). Scaling theories of polymer solutions and brushes[102,110,111] allowed describing of the structure of micelles in dilute and semi-dilute solutions. The original scaling models of crew-cut[112] and starlike aggregates[113–115] utilized the blob concepts to envision the soluble corona of a micelle as a densely packed system of concentration blobs with almost constant (crew-cut micelle) or increasing (starlike micelle) size to the periphery of the corona, and the core densely packed with thermal blobs. Because a soluble corona prevents precipitation of the block copolymer in sediment, micelles could remain thermodynamically and aggregatively stable in a wide range of solution concentrations by adjusting their size, shape, and packing.[116–119]

The scaling model of spherical micelles with bb blocks[90] is based on subdivision of the bottlebrush free energy into the "internal" free energy of the superblobs and that of superblob–superblob interactions. The former contribution accounts for monomer–monomer interactions within superblobs (on length scales $<D$) and is much larger than k_BT per superblob. The latter contribution governs the chain conformations on length scales $>D$, and approaches k_BT per superblob only in strongly stretched or condensed chains of superblobs. If the structure of superblobs is unperturbed in the core and the corona of micelles, or all of the corona superblobs are compressed equally (as in, *e.g.* a semi-dilute solution of bb polymers), the "internal" contribution does not manifest itself in micellization of diblock copolymer with bb blocks. However, compression of the core superblobs or selective perturbation of the corona superblobs is prevented by the increase in the "internal" free energy, giving

rise to micelles with strongly stretched backbones at relatively small DPs of the blocks.

The theoretical models provide the asymptotic power law dependences for micelle equilibrium parameters (aggregation number, core and corona sizes, critical micelle concentration (cmc) corresponding to the onset of micellization in the block copolymer solution) as a function of molecular weights of the blocks and solvent selectivity, and serve as guidelines to rationalize the experimental data. In addition to the scaling models,[90] a self-consistent field (SCF) approach to polymer micelles[91] allowed incorporation of moderately good solvent conditions (justified for semi-flexible corona blocks) and examination of the crossovers between different regimes. As it followed from these studies, the self-assemblies with branched (starlike and comb-shaped) blocks exhibit a more diverse behavior compared to micelles formed by diblock AB copolymers with linear blocks.[113,114] To highlight this difference, we review here the equilibrium features of micelles formed by the diblock AB copolymer that comprises bottlebrush (bb) blocks with long backbones.

Diblock copolymer molecule AB consists of two chemically different bb blocks, Fig. 7. Block i = A, B has degree of polymerization (DP) of backbone M_i, and DPs n_i and m_i of the side chains and spacer separating neighboring grafting points ($n_i/m_i \gg 1$, the bottlebrush regime) with total DP $N_i = M_i(1 + n_i/m_i)$. The backbone and the side chains in both blocks are assumed to be intrinsically flexible, that is, the monomer unit size a (the same for both blocks), is on the order of the Kuhn segment length. The solvent is assumed to be poor for block B and athermal ($\nu = 3/5$) or theta-solvent ($\nu = 1/2$) for block A. Below we focus on densely grafted bb blocks with $m_i \simeq 1$, i = A, B that have been investigated in many experiments.[78–85]

Soluble block A is envisioned as a wormlike chain with thickness $D_A \simeq a n_A^{2\nu/(\nu+1)}$ (*i.e.*, with superblob size given by eqn (2) with $n = n_A$ and $m = m_A \sim 1$) and the effective persistence length $l_{p,A} \simeq D_A$. It gives rise to $N_{AS} = aM_A/D_A$ of superblobs that are essentially impermeable due to the elastic stretching of side chains normally to the backbone. The average size H_u of a single block A is governed by repulsive superblob–superblob interactions, and exhibits the excluded volume statistics on length scales larger than D_A. That is,

$$H_u \simeq D_A N_{AS}^{3/5} \simeq a^{3/5} D_A^{2/5} M_A^{3/5} \quad (17)$$

In the case of short (oligomeric) side chains with $n_A \simeq 1$, and $D_A \simeq a$, bb block A is treated as linear with DP N_A with

$$H_u \simeq a N_A^{\nu} \quad (18)$$

Insoluble block B has superblob size $D_B \approx a(n_B/\tau_B)^{1/2}$ with the side chains stretched normally to the backbone up to $\tau_B \lesssim 1$, where τ_B is relative deviation from the theta-temperature (measure of the thermodynamic quality of poor solvent) for monomer units of the block B. The number of superblobs in block B is $N_{BS} = aM_B/D_B$. In a selective solvent, insoluble block B condenses in a globule with radius

$$R_u \simeq a(N_B/\tau_B)^{1/3}, \quad (19)$$

while block A ensures the solubility of block copolymer in the solution.

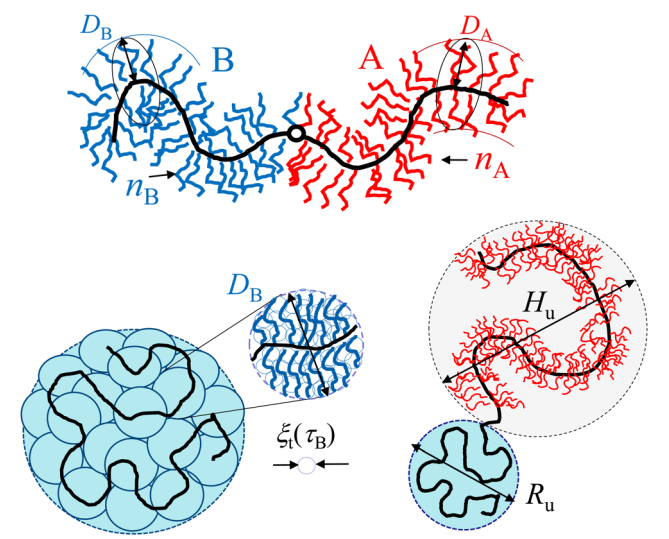

Fig. 7 Schematics of AB block copolymer with bottlebrush blocks, $m_A \cong m_B \cong 1$. Backbones in both blocks are indicated by thick black lines.

4.1 Starlike micelles

The equilibrium aggregation number Q in a spherical micelle with flexible core and corona blocks is specified by optimizing the free energy F per molecule. In the narrow interface approximation, F comprises the free energies F_A and F_B of blocks A and B, and the surface free energy F_{surf} at the core/corona interface,

$$F = F_A + F_B + F_{surf} \quad (20)$$

Based on the blob concepts,[90] the free energy F_A per block A in the corona envisioned as a spherical brush with thickness

$$H \simeq D_A Q^{1/5} N_{AS}^{3/5} \simeq a^{3/5} D_A^{2/5} Q^{1/5} M_A^{3/5} \quad (21)$$

circumventing the core with radius $R \simeq a(QN_B/\tau_B)^{1/3}$ can be evaluated as the total number of concentration blobs (with size $\xi(r) \simeq r/Q^{1/2}$ and the free energy $\simeq k_BT$ per each blob), formed by the chains of superblobs with size D_A, see Fig. 8,

$$\frac{F_A}{k_BT} \simeq Q^{1/2} \ln\left(\frac{H}{R}\right) \quad (22)$$

The Q-dependent elastic contribution per block B is specified as for a Gaussian chain of superblobs with size D_B,

$$\frac{F_B}{k_BT} \simeq \frac{R^2}{D_B^2 N_{BS}} \simeq Q^{2/3} N_B^{-1/3} n_B^{1/2} \tau_B^{-1/6} \quad (23)$$

The surface free energy F_{surf} per molecule is evaluated as the number of the thermal blobs with size $\xi_{t,B} \simeq a\tau_B^{-1}$ per surface area $s \simeq R^2/Q$,

$$\frac{F_{surf}}{k_BT} \simeq \frac{s}{\xi_{t,B}^2} \simeq \frac{\tau_B^{4/3} N_B^{2/3}}{Q^{1/3}} \quad (24)$$

Minimization of F with respect to Q reduces to balance $F_A \simeq F_{surf}$, to provide the power law dependence for aggregation

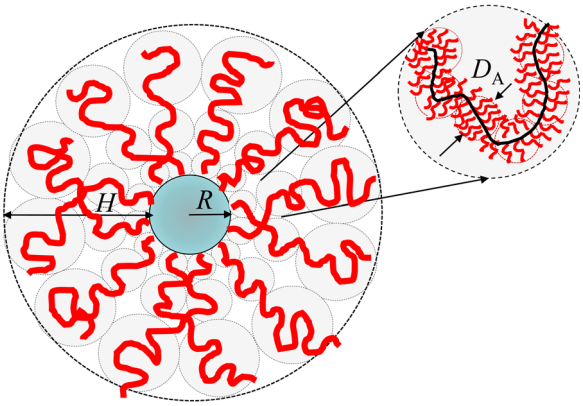

Fig. 8 Blob structure of starlike micelle with aggregation number Q (regime ST in diagram of states in Fig. 9). Backbones and side chains in the corona blocks are indicated in black and red, respectively. Densely packed, increasing to the corona periphery concentration blobs with size $\xi(r) \cong rQ^{-1/2}$ are indicated in light grey.

number,

$$Q_{0,ST} \simeq \frac{\tau_B^{8/5} N_B^{4/5}}{\ln^{6/5}(H_0/R_0)} \tag{25}$$

with subscripts "0" indicating equilibrium values of the micelle parameters and "ST" indicating starlike shape of micelles. Notably, at fixed DP N_B of the condensing block B, $Q_{0,ST} \simeq \tau_B^{8/5} N_B^{4/5}$ and $R_{0,ST} \simeq a(Q_{0,ST} N_B/\tau_B)^{1/3} \tau_B^{1/5} N_B^{3/5}$ are weakly affected (*via* the logarithmic prefactors) by bb branching of both blocks A and B. However, the corona thickness $H_{0,ST}$ (eqn (21) with $Q = Q_{0,ST}$) depends on DP n_A of the side chain in soluble block A. Different modes of branching, *e.g.* an increase in n_A at fixed $N_A = M_A n_A$ or fixed M_A would lead to the respective decrease or increase in the corona thickness, $H_{0,ST}$, at almost constant value of the aggregation number, $Q_{0,ST}$. The effect of n_B is weak, but this changes upon decreasing N_B.

For bb block copolymers with strongly branched block B ($D_B \geq D_A$) a decrease in N_B leads to the decrease in area $s_0 \simeq R_{0,ST}^2/Q_{0,ST} \sim a^2 \tau_B^{-6/5} N_B^{2/5}$ of the core/corona interface per molecule. At $N_B = N_B^* \simeq \tau_B^3 (D_B/a)^5$ or, equivalently,

$$M_B = M_B^* \simeq \tau_B^2 (D_B/a)^3,$$

area s_0 decreases down to the superblob cross-section, D_B^2, and the backbone of block B approaches limiting extension,

$$R_{0,ST}^* \simeq D_B N_{BS} \sim a M_B \tag{26}$$

Further decrease in s_0 would perturb the structure of superblobs in the micelle core, leading to a strong increase in the free energy per chain. As a result, starlike micelles formed by bb block copolymers with $M_B < M_B^*$ retain area $s_0 \simeq D_B^2$ of the core/corona interface per molecule, and exhibit strongly stretched backbones that specifies the micelle equilibrium aggregation number as

$$Q_{0,ST_B} \simeq \left(\frac{N_B}{\tau_B}\right)^2 \left(\frac{a}{D_B}\right)^6 \simeq M_B^2 \left(\frac{a}{D_B}\right)^2 \text{ if } M_B < M_B^* \simeq \tau_B^2 (D_B/a)^3, \tag{27}$$

while the corona thickness (eqn (21) with $Q = Q_{0,STB}$) is given by

$$H_{0,ST_B} \simeq a\left(\frac{D_A}{D_B}\right)^{2/5} M_A^{3/5} M_B^{2/5} < a M_A \tag{28}$$

Here, subscript "ST_B" indicates strong stretching of backbones of the core-forming blocks.

The micelles with strongly elongated backbones in blocks B (termed also core-stretched micelles) disintegrate into unimers ($Q_{0,STB} \simeq 1$) when block B reduces to a single superblob, *i.e.*, $M_B = M_B^{**} \simeq D_B/a$, and the corona thickness $H_{0,STB}$ reduces to H_u in eqn (17).

In the opposite case of strongly branched bb block A with $D_A > D_B$, perturbation of the corona superblobs adjacent to the core of the micelle leads to several additional regimes of micelle behavior[90] including ones with strongly stretched backbones in both blocks.

4.2 Crew-cut micelles

Starlike micelles with $H \geq R$ transform into crew-cut aggregates with $H \leq R$, when $H \simeq R$. In a crew-cut micelle, the corona is planar-like, and its conformational free energy F_A can be obtained from the free energy $F/k_BT \simeq N_A(s/a^2)^{-\frac{1}{2\nu}}$ in a planar brush of linear chains[110] with DP N_A and grafting area s by substituting $a \to D_A$, $N_A \to N_{AS} = aM_A/D_A$, and $\nu = 3/5$, to give

$$\frac{F_A}{k_BT} \simeq M_A \left(\frac{D_A}{a}\right)^{2/3} \left(\frac{a^2}{s}\right)^{5/6} \tag{29}$$

The expressions for F_B and F_{surf} (eqn (23) and (24)) remain unchanged. By using the packing condition, $Q \simeq N_B^2 \tau_B^{-2} s^{-3}$ and minimizing the free energy F per chain with respect to Q (or s), one finds the aggregation number in micelles formed by AB copolymer with long bb blocks,

$$Q_{0,CC} \simeq \frac{R^2}{s} \simeq \frac{M_B^2 \tau_B^{36/11}}{M_A^{18/11}} \left(\frac{D_B}{a}\right)^4 \left(\frac{D_A}{a}\right)^{-12/11} \tag{30}$$

with subscript "CC" indicating the micelle crew-cut shape. Similarly to starlike micelles, a decrease in $M_B < M_B^*$ leads to strong stretching of the backbones in both blocks, and changes the values of exponents in eqn (30) leading to a number of novel subregimes.[90] Notably, scaling models do not predict micelles with strongly stretched linear blocks.[113,114]

To highlight the effect of bb branching we compare the scaling-type diagrams in M_A, M_B coordinates for the case of linear (Fig. 9a) and bb branched (Fig. 9b) blocks with equal thicknesses, $D_A = D_B = D$. Block copolymers with linear blocks give rise to either starlike (regime ST) or crew-cut micelles (regime CC) with both blocks remaining moderately stretched prior to disintegration in unimers. Crew-cut micelles transform in cylindrical aggregates and lamellae with further precipitation in the sediment (shaded areas in Fig. 9) upon decreasing M_A. The stability range of cylindrical morphology is not distinguished in scaling terms (*i.e.*, the boundaries for cylindrical micelles obey the same power law dependences on the system parameters and differ only in the numerical prefactors), and is indicated by the dotted line in Fig. 9a.[119]

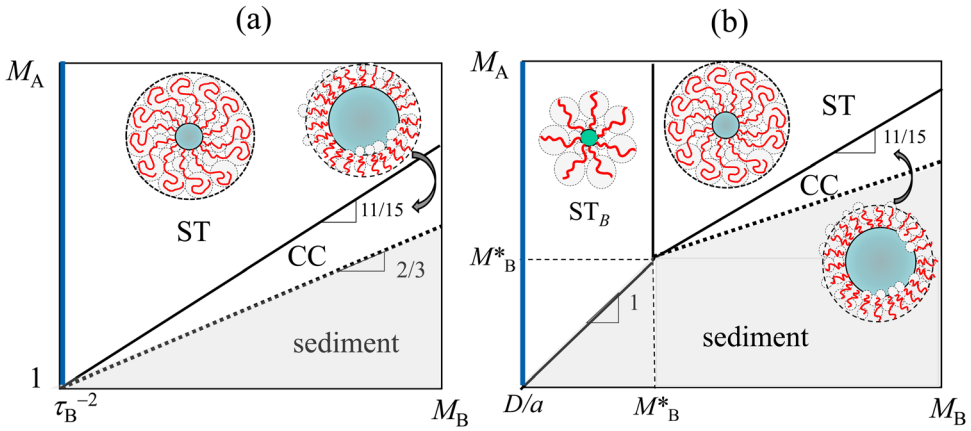

Fig. 9 Scaling-type diagrams of states in M_A, M_B coordinates for AB diblock copolymer with linear blocks (a) and bb blocks with $D_A = D_B = D$ (b) in dilute solution, $\nu = 3/5$. Starlike and crew-cut micelles are found in regions ST and CC, respectively, starlike micelles with strongly stretched core block are located in region ST_B, $M^*_B = \tau_B(D/a)^3$. Slopes of the ST–CC boundaries are indicated. At vertical blue lines $M_B \cong \tau_B{}^{-2}$ (a) and $M_B \cong D/a$ (b) micelles disintegrate into unimers. Dotted line with slope 2/3 marks the stability corridor of cylindrical micelles.

In contrast, block copolymers with bb blocks give rise to the additional regime ST_B in which the core-forming blocks B are strongly stretched approaching limiting extension, $R_{0,STB} \simeq aM_B$. Disintegration of core-stretched micelles into unimers occurs at larger values of $M_B = M^{**}_B \simeq D/a$ compared to micelles with linear blocks. The boundary between ST and CC regimes exhibits the same value of exponent (11/15) for diblock copolymers with long blocks $(M_A, M_B > M^*_B)$ but is shifted up to larger values of M_A and M_B. Starlike core-stretched micelles in regime ST_B transform into crew-cut aggregates when $M_A \simeq M_B$ (boundary line with slope 1 in Fig. 9b) at which the backbones in corona blocks A approach maximal extension, $H \simeq aM_A$. In the vicinity of this boundary crew-cut micelles with strongly stretched core and corona blocks precipitate in the sediment.

Similar to the case of linear block copolymers,[115,119–121] the critical micelle concentration (cmc) in a dilute solution is governed mostly by DP N_B of insoluble block B while the dependence on DP N_A of soluble block A is weak. In scaling terms,[90] cmc for starlike micelles is determined by the surface free energy of a unimer with condensed block B as $\ln \text{cmc} \simeq -(\tau_B{}^2 N_B)^{2/3} + F_A/k_BT \simeq -(\tau_B{}^2 N_B)^{2/3}$, and thereby is not very sensitive to bb branching of block B at fixed total DP $N_B = M_B n_B$.

Micellization of diblock copolymers with bb blocks was experimentally examined in a number of studies,[78–85] and the extended conformations of backbones were detected. However, AB copolymers with water-soluble side chains in the corona block, *e.g.*, PACMO,[81] PEO,[80] exhibit poor consistency with the theoretical models. Micelles soluble in organic solvents typically demonstrate better agreement, although up to now systematic variations in the system parameters are rare.[82,85] The experimental samples are typically found either close to the boundary between starlike and crew-cut micelles,[85] or the side chains are too short. A recent study[82] provided systematic data for the equilibrium parameters of spherical micelles in 1 wt% solution of poly(5-perfluorooctyl norbornene-*b*-*N*-cyclohexyl-*exo*-norbornene-5, 6-dicarboxyimide) (PF-*b*-PC) block copolymer in THF (poor solvent for PF block). The PF block contained densely grafted short side chains (C_8F_{17}) while DP M_B of this block, and DP N_A of the linear PC block were varied. In scaling terms, short stiff side chains on the norbornene backbone constitute oligomers with $n_B \simeq 1$. Therefore, one would expect that exponents in the power law dependences of R and H might be close to the exponents for linear AB polymers.

In Fig. 10, the radius R of the micelle core[82] is presented as a function of DP M_B of the PF block for two molar masses of corona block A, 50 kDa (red triangles) and 300 kDa (blue squares) in log–log coordinates. According to the scaling model, $R \sim N_B{}^{3/5}$ depends on N_A only logarithmically, and slope 3/5 is indicated by a single dashed line for both series (with 50 kDa and 300 kDa for block A). We also indicated slope 1 with a solid line for each series (red for triangles and blue for squares) predicted for core-stretched (ST_B) micelles.

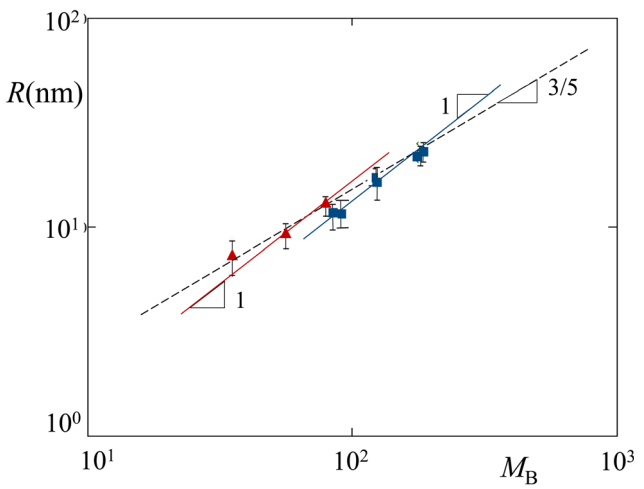

Fig. 10 Core radius R as a function of DP M_B of the backbone in the core-forming PF block for two molecular masses of PC block A, M_A = 50 kD (triangles) and M_A = 300 kD (squares).[82] Dashed and solid lines with slopes 3/5 and 1 correspond to conventional starlike (ST) and core-stretched (ST_B) micelles, respectively.

While slope 1 is plausible for each of the series, and the shift down of the blue line with respect to the red one could be due to the logarithmic prefactor comprising M_A, the exponent 3/5 still fits better the whole set of data. Clearly, more experiments with systematically varied lengths of flexible side chains and backbones are required to confront the theoretical predictions.

An increase in the solution concentration c leads to overlap and concomitant contraction of the micelle's coronas. As was demonstrated for linear–linear AB block copolymers,[113,114] in semi-dilute solutions starlike micelles organize in densely packed arrays, so that their dimensions exhibit quasi-globular dependence, $H \simeq a(QN_A/c)^{1/3}$, with c-dependent aggregation number $Q(c)$ up to $c \simeq 1$. Similar quasi-globular regimes are expected for micelles with bb blocks due to the same physical reason – elastic stretching of the corona blocks preventing essential interpenetration of neighboring micelles. In these regimes, the ratio of the corona thickness $H \simeq a(QN_A/c)^{1/3}$ to the core radius $R \simeq a(QN_B/\tau_B)^{1/3}$ decreases as $H/R \sim c^{-1/3}$ irrespective of specific architectures of blocks A and B, making R and H closer in size upon increasing c. In concentrated solutions, the equilibrium dimensions of micelles attain the molecular mass dependences characteristic for melts of microphase segregated diblock copolymers, $R \sim H \sim N^{2/3}$. Depending on selectivity of the solvent, self-assembled aggregates of AB block copolymers can retain their shape or undergo morphological transformations[86,100,116] upon increasing solution concentration c.

5 Melt of block copolymer with branched blocks

Microphase segregated melts of block copolymers with branched blocks have been extensively studied both experimentally[70–77] and theoretically.[59–69] In the strong segregation limit, conformations of the blocks could be described using polymer brush models. That is, a narrow A/B interface allows for assimilation of the conformational free energies of the blocks in inner (B) and outer (A) domains to dry concave and convex polymer brushes, respectively. The free energies F_A and F_B can be calculated analytically using the strong stretching self-consistent field (SS-SCF) approximation originally proposed for linear block copolymers by Semenov[55] and generalized later for dendron brushes by Pickett[122,123] and for brushes formed by macromolecules of arbitrary regularly branched topology in ref. 124–126.

In the simplest case of equally flexible blocks with the same size of monomer units, a, the SS-SCF approach specifies molecular parabolic potentials $U_j(z)$ (j = A, B) acting in the domain with size d_j as a function of distance z from the A/B interface,

$$\frac{U_j(z)}{k_B T} = \frac{3\pi^2}{8N_j^2 a^2}\eta_j(d_j^2 - z^2) \quad (31)$$

The architecture-dependent topological ratio η_j allows for quantification of the increase in the elastic free energy of branched block j with DP N_j compared to linear block with the same N_j. For polymer with branched architecture, η is calculated by using the conditions of length conservation for the segments between branching units, and by balancing the elastic forces in all branching units of the macromolecule.[125] Although parabolic molecular potential U_A produces the so-called dead zones (*i.e.*, regions depleted of the chain free ends) in the convex matrix, and thereby slightly underestimates the elastic free energy F_A, the SS-SCF approach can still be implemented to establish basic morphological features of microphase segregated melt of branched block copolymers. Extension of the SS-SCF theory to different sizes of monomer units and Kuhn segments of the blocks is straightforward and can be found elsewhere.[64]

Comblike (cl) polymers are conventionally distinguished from bottlebrush (bb) polymers *via* conformations of spacers between neighboring side chains in melts. Spacers with DP $m \gtrsim n^{1/2}$ of cl polymers with DP n of side chains exhibit Gaussian conformations in melts, while in bb polymers with $m \leq n^{1/2}$ backbones in melts are locally stretched. The parabolic molecular potential in eqn (31) with topological ratio

$$\eta_{cl} = \left(1 + \frac{n}{m}\right)^{1/2} \quad (32)$$

can be directly applied to brushes of cl polymers with backbones that start to elongate upon increasing the grafting density of side chains. For bb polymers with locally stretched backbones introduction of superblobs with size $D \simeq an^{1/2}$ as bb chain impermeable elements leads to modification of η as[64]

$$\eta_{bb} \simeq n^{1/4} \quad (33)$$

with the numerical coefficient on the order of unity.

Equilibrium morphology of the microphase segregated domains can be found from the condition

$$F^{(i)}(s_{eq}) \rightarrow \min\{i\}, \quad (34)$$

where index i = 1 refers to lamellae, i = 2 to cylindrical and i = 3 to spherical domains, and the free energy $F^{(i)}(s)$ per block copolymer chain in the superstructure with morphology i,

$$F^{(i)}(s) = F_A^{(i)}(s) + F_B^{(i)}(s) + F_{A/B}^{(i)}(s) \quad (35)$$

comprises respective conformational entropies of the stretched blocks A and B, and the excess free energy of the A/B interface between domains and the matrix, and has to be minimized with respect to the interfacial area s per molecule. While in melts of linear–linear block copolymers the segregated domains are formed by the minority block and embedded into the continuous matrix formed by the majority block, this might not be the case if the copolymer blocks are asymmetrically branched.[63,64]

In Fig. 11 we present the unified morphology diagram of microphase segregated melt of diblock copolymer with long block backbones M_j in the η_A/η_B, $f_A = N_A/(N_A + N_B)$ coordinates constructed in the SS-SCF approximation for both blocks. The diagram incorporates AB copolymers that contain cl or bb blocks and their combinations (with formulation of the topological ratios η_B and η_A according to eqn (32) and (33)). Major morphologies (spheres S, S′, cylinders C, C′, and lamellae L)

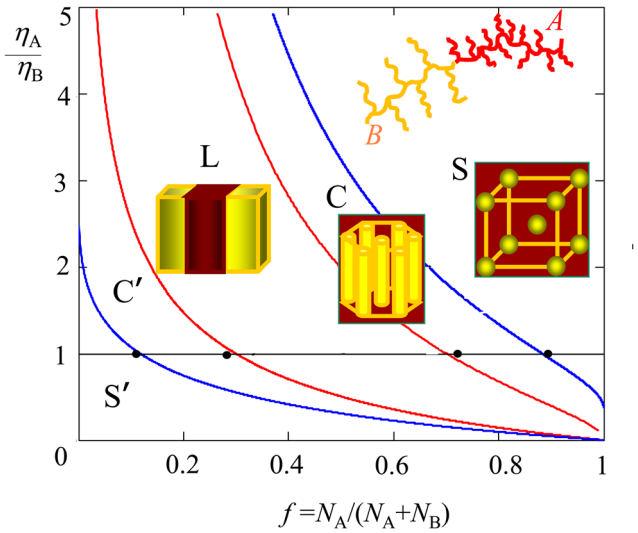

Fig. 11 Morphology diagram of microphase segregated melt of AB block copolymer with branched blocks.

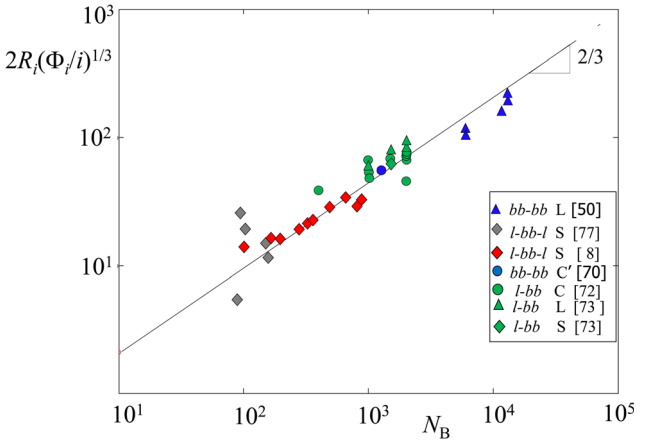

Fig. 12 Power law dependence for normalized domain radius R_i as a function of N_B. Copolymers BAB were treated as diblock copolymers A(B/2). Shape and color of different symbols are indicated in the inset with references to the experimental data.

are separated by binodals. The more complex *e.g.* double gyroid structures are not included here. The *X*-axis with $\eta_A/\eta_B = 1$ corresponds to symmetrically branched blocks including linear blocks with $\eta_A = \eta_B = 1$. Black dots on the *X*-axis indicate the transition compositions predicted by Semenov's model[55] for linear block copolymers in the strong segregation limit. As is seen in Fig. 11, an increase in branching asymmetry η_A/η_B leads to a significant shift of binodals to smaller values of f_A and stabilization of the spherical morphology S.

Among predictions of the analytical SS-SCF model[64] is the universal dependence for radius R_i of the domains formed by block B in spherical ($i = 1$), cylindrical ($i = 2$) and lamellar ($i = 3$) morphologies,

$$2R_i\left(\frac{\eta_A^2 g_i\left(\frac{f_A}{1-f_A}\right)\beta + \eta_B^2 b_i}{i}\right)^{1/3} = KN_B^{2/3} \qquad (36)$$

with the geometry- and composition-dependent functions g_i, the numerical coefficients b_i, and prefactor $K \simeq 1$ which is independent of the degree of polymerization N_B of the domain-forming block or the domain morphology i. Because the topological ratio depends only on how the chain segments are connected in a branched polymer, η_j does not depend on DPs of the blocks (N_j). Therefore the equilibrium dimensions of the domains obey the same molecular weight dependences, $R_i \sim N_B^{2/3}$, as for linear diblock copolymers. In Fig. 12 eqn (36) is applied to the experimental data for block copolymers with different lengths and domain morphologies.[8,50,70,72,73,77] As seen in Fig. 12, exponent 2/3 is consistent with the majority of data points except for strongly scattered data for relatively small N_B.

In the framework of parabolic molecular potential, the side chains in microphase segregated domains are weakly stretched in the direction perpendicular to the domain boundaries in contrast to a much stronger elongation of the backbones. The distribution of backbone tension in brushes of cl and bb polymers is nonuniform: it is maximal near the boundary between the domains and gradually reduces to the free end of the backbone. Only close to the backbone free end do the side chains exhibit elastic stretching comparable to the local stretching of the backbone. Notably, such behavior of the side chains is similar to that of short linear polymers inserted at different positions in the brush formed by long polymers.[127] That is, the side chains near the A/B boundary are almost unstretched, their elongation increases with distance z from the surface, and reaches maximum at the backbone free end. The computer simulations of tension distribution in brushes of moderately stretched bottlebrushes[128] are consistent with this picture.

Overall, microphase segregated melts of block copolymers with branched blocks demonstrate a more complex organization compared to linear counterparts. For example, symmetric cl–cl and bb–bb block copolymers with variable length M of backbone can undergo conformational transitions between the regimes of miktostar (short backbone) to conventional bottlebrushes (long backbone).[62] The power law dependences for lamellar spacing in these two regimes are different, and no analog of this transition is feasible in linear diblock copolymers.

5.1 ABA triblock copolymers

Microphase segregated melts of triblock copolymers BAB differ from AB diblock copolymers due to forming of loops and bridges connecting neighboring B-domains.[75] However, in the strong segregation limit, the equilibrium parameters of the domains formed by triblock copolymer BAB with DP $2N_A$ of the central block are expected to obey the same power law dependences as for AB diblock copolymers with DP N_A of the central block A. This commonly used approximation is exploited, in particular, in Fig. 11, in which the value of exponent (2/3) in the dependence $R_i(N_B)$ is checked for a set of diblock AB and triblock BAB copolymers forming different morphologies ($i = 1, 2, 3$).

An important characteristic of the self-assembling triblock copolymer gels and elastomers is fraction X_{bridge} of bridges connecting neighboring B-domains. The latter determines the elastic response to deformation and can be manipulated by varying the architecture of the blocks. In the case of microphase segregated lamellar ($i = 1$) domains,[66] fraction X_{bridge} of bridges could be evaluated analytically using the parabolic molecular potentials U_j (eqn (31)). In this approach, fraction X_{bridge} of bridges formed by the central A-block of BAB triblock copolymer is estimated from the equilibrium properties of lamellae formed by diblock B(A/2) block copolymer. That is, A-loop is modelled as two tethered subchains with DP N_A with unrestricted free ends, while the middle point of A-bridge is fixed at the boundary of the Wigner–Seitz cell.

The numerical calculations performed using Scheutjens–Fleer self-consistent field method[129] for solvent-free planar layers formed by loops and bridges of linear and comblike polymers[66] were in accord with the analytical model in eligible ranges of the system parameters. In particular, branching of the central (A) or of all the blocks in BAB copolymer lead to the decrease in X_{bridge} compared to BAB triblock with linear blocks of similar DPs. Symmetric comblike branching of A and B blocks lead to a stronger decrease in X_{bridge} compared to triblock with branched A and linear blocks B. Branching of B-blocks with $\eta_B > \eta_A$ increased X_{bridge} compared to linear B-block. An increase in the degree of branching of A-block leads to the decrease in X_{bridge} with a concomitant increase in the network shear modulus $G_{melt} \sim \eta_A^2 N_B^{-2/3}$.

In other morphologies of microphase segregated BAB melts ($i = 2, 3$) fraction X_{bridge} of bridges could be also estimated analytically[67] or numerically.[130] In the former case, account of the dead zones in the A-matrix inverted the decrease in X_{bridge} as a function of the copolymer composition, $f_A = N_A/(N_A + N_B)$, leading to the approach to $X_{bridge} \simeq 0.5$ from below, and thereby indicating the decrease in the difference between elastic free energies of loops and bridges. However, MD simulations[130] indicated $X_{bridge} > 0.5$ in melts of triblock BAB copolymers with spherical B-domains and short side chains in the central bb block. This numerical discrepancy could arise due to the decreased stretching of bridges in the interdomain space compared to the Wigner–Seitz cell model implemented in the analytical theory.

6 Conclusions and perspectives

As discussed in this review, specific molecular architecture and strong intramolecular interactions lead to numerous features of bottlebrush polymer solutions, melts, networks, and colloidal nanostructures that distinguish them from linear counterparts.

At present, a general understanding of bottlebrushes with a basic set of independently controlled architectural parameters $\{M,n,m\}$ is achieved in solutions. It was demonstrated theoretically that interactions between side chains lead to stiffening of the bottlebrush on the length scale comparable to the dimensions of extended side chains, and this prediction is in good agreement with the results of computer simulations and scattering experiments. As a result, the elastic modulus of bb polymer is significantly smaller compared to that of its ''bare'' backbone. The ''softening'' effect is expected to occur at any grafting density of the side chains. However, at moderate grafting density at which the backbone spacers in an unperturbed bottlebrush are not fully extended, the force–extension curves acquire a characteristic sigmoidal shape with a sharp increase in the restoring force at the end-to-end distance corresponding to full stretching of the chain of ''superblobs'' – chain segments with size equal to bb thickness D.

An increase in the solution concentration c beyond the overlap threshold leads to screening of intramolecular interactions on progressively decreasing length scale and the corresponding increase in the chain elasticity that gives rise to a number of regimes with different power law dependences for static and dynamic properties on the solution concentration, c. An increase in the branching parameter $n/m \gg 1$ leads to widening of specific for bb polymer regimes, whereas at $n/m \sim 1$ the behavior of the solution of linear chains is recovered.

Based on the scaling description of solutions of bb polymers, the theory enables unravelling of specific properties of the ''haired'' gels comprising bottlebrush strands. It is predicted that the swelling ratio of the haired gels is controlled primarily by the DP of the main chains of the strands, whereas the dependence on the DP and grafting density of the side chains is weak. This prediction is in agreement with the experimental data. The theory also predicts a non-monotonic dependence of the osmotic modulus of ''haired'' gels on DP of the side chains with a minimum corresponding to the overlap threshold of the side chains emanating from different strands.

Self-organization of block copolymers with bb blocks in selective solvents and in melts exhibits a number of distinctive features compared to linear–linear block copolymers. An increasing number of monomer units in the side chains (*i.e.*, an increase in the branching parameter n/m) leads to the decrease in ratio of the main chain length (along which the elastic tension propagates) to the block volume. In the case of the solution self-assembly, bb branching of soluble blocks leads to a decrease in the aggregation number and overall size of the micelles with a concomitant weak increase in cmc, as compared to linear diblock copolymers with the same DP of the soluble block. The bb block copolymers with a relatively short main chain in the insoluble block form micelles in which backbones of bb blocks in the core are strongly stretched approaching the limit of extensibility. This leads to novel power law dependences for the structural properties of the core-stretched micelles.

Morphologies of nanodomains in microphase segregated melts of block copolymers with strongly incompatible bb blocks can be efficiently tuned by changing the degrees of branching at constant volume fractions of the respective blocks. This leads to qualitatively new features in the morphological phase diagram: for instance, a strongly branched minority block may form a continuous matrix with embedded spherical or cylindrical domains of the majority component

which is impossible for linear–linear block copolymers. The theoretically predicted morphological phase diagram accounting for bb branching of blocks[64] is in accord with the available up to date experimental data for three basic geometries (spheres, cylinders, lamellae).

At the same time our understanding of static and dynamic properties of solutions and melts of bottlebrush block copolymers is still incomplete and a number of challenges remain:

While scaling analysis has been applied to study dynamics of bb networks and melts,[97,98,131] and gelation of bb polymers,[25,26] a comprehensive theoretical description of the effect of bb branching on dynamic properties in solution is currently lacking. Furthermore, the effect of the bb branching on the ability of the polymer to crystallize is far from being understood, although it is highly relevant for the development of energy-storage devices.

The effects of intramolecular ionic interactions and their impact on the rigidity and extensional elasticity of bb polymers with ionically charged side chains have been addressed just partially.[48,132] Self-assembly of amphiphilic block copolymers with one hydrophobic block and another ionically charged (strong or weak polyelectrolyte) bb block has not been yet explored.

An intriguing feature of the bottlebrush (co)polymers is that they closely mimic natural glycoproteins (*e.g.* lubricin and mucins) or proteoglycans (*e.g.* aggrecan) comprising polysaccharide chains terminally attached to the backbone formed by the core protein. While aggrecan (in complex with hyaluronian acid) is an important constituent of the articular cartilage,[133] it is believed that interfacial layers formed by lubricin attached to the cartilage in the joints are responsible for dramatic reduction of intra-joint friction.[134] Such lubricating property of synthetic bottlebrushes anchored at sliding surfaces in aqueous media has been demonstrated experimentally.[135,136] Among possible explanations of this effect is the theoretically predicted[137] narrowing of the interpenetration zone between apposing brushes formed by branched polymers. More theoretical studies with an explicit account of the bb architecture of the end-tethered macromolecules could provide better insights into biolubrication and allow for design of novel biomimetic materials.

Glossary

a	Monomer unit length
c	Solution concentration (monomer number density)
d	Domain size in the microphase segregated melt of block copolymers
D	Cross-sectional dimensions of the molecular brush (the superblob size)
f_A	Volume fraction of the block A in the copolymer
F	Helmholtz free energy
G	Osmotic modulus of the gel
h	End-to-end distance of a spacer
H	Thickness of the micellar corona
H_u	Size of the soluble block A in the block copolymer in the unimer state
L	The apparent contour length of the molecular brush
l_p	The apparent persistence length of the molecular brush
m	Polymerization degree of a spacer
M	Polymerization degree of the main chain
n	Polymerization degree of a side chain
N	Total degree of polymerization of the molecular brush
N_{AS}, N_{BS}	Numbers of superblobs in the bottlebrush blocks A and B, respectively
P	Total number of side chains in the molecular brush
Q	Number of block copolymers in a micelle (aggregation number)
R_{eq}	Equilibrium dimensions of the molecular brush
R_{end}	End-to-end distance of the main chain
R_u	Size of the individual collapsed insoluble block B
s_{eq}	Equilibrium surface area of the A/B interface per block copolymer
U	Self-consistent molecular potential
V	Volume of the swollen gel
V_{dry}	Volume of the dry (solvent-free) gel
ν	The Flory exponent
η	The topological ratio
ρ	Radial distance from the backbone
ξ	The concentration blob size
τ	Relative deviation from the theta-point (reduced temperature)

Conflicts of interest

There are no conflicts of interest to declare.

Acknowledgements

This work was supported by the Russian Science Foundation, grant 20-13-00270.

References

1 S. S. Sheiko, B. S. Sumerlin and K. Matyjaszewski, Cylindrical molecular brushes: Synthesis, characterization and properties, *Prog. Polym. Sci.*, 2008, **33**, 759–785.
2 R. Verduzco, X. Li, S. L. Pesek and G. E. Stein, Structure, function, self-assembly of bottlebrush copolymers, *Chem. Soc. Rev.*, 2015, **44**, 2405–2420.
3 M. Müllner and A. H. E. Müller, Cylindrical polymer brushes – anisotropic building blocks, unimolecular templates and particulate nanocarriers, *Polymer*, 2016, **98**, 389–401.
4 J. Rzayev, Molecular Bottlebrushes: New Opportunities in Nanomaterials Fabrication, *ACS Macro Lett.*, 2012, **1**, 1146–1149.
5 X. Li, S. L. Prukop, S. L. Biswal and R. Verduzco, Surface Properties of Bottlebrush Polymer Thin Films, *Macromolecules*, 2012, **45**(17), 7118–7127.

6 H. Liang, S. S. Sheiko and A. V. Dobrynin, Supersoft Polymer Networks with Brushlike Strands, *Macromolecules*, 2018, **51**, 638–645.

7 J. Yuan, A. H. E. Müller, K. Matyjaszewski and S. Sheiko, in *Polymer Science: A Comprehensive Reference*, ed.-in-chief K. Matyjaszewski and M. Möller, Elsevier, Amsterdam, 2012.

8 C. Clair, A. Lallam, M. Rosenthal, M. Sztucki, M. Vatankhah-Varnosfaderani, A. N. Keith, Y. Cong, H. Liang, A. V. Dobrynin, S. S. Sheiko and D. A. Ivanov, Strained Bottlebrushes in Super-Soft Physical Networks, *ACS Macro Lett.*, 2019, **8**, 530–534.

9 G. Xie, M. R. Martinez, M. Olszewski, S. S. Sheiko and K. Matyjaszewski, Molecular Bottlebrushes as Novel Materials, *Biomacromolecules*, 2019, **20**(1), 27–54.

10 S. Rathgeber, T. Pakula, A. Wilk, K. Matyjaszewski and K. L. Beers, On the shape of bottle-brush macromolecules: systematic variation of architectural parameters, *J. Chem. Phys.*, 2005, **122**(12), 124904.

11 Z. Li, M. Tang, S. Liang, M. Zhang, G. M. Biesold, Y. He, S.-M. Hao, W. Choi, Y. Liu, J. Peng and Z. Lin., Bottlebrush polymers: From controlled synthesis, self-assembly, properties to applications, *Prog. Polym. Sci.*, 2021, **116**, 101387.

12 A. Kerr, M. Hartlieb, J. Sanchis, T. Smith and S. Perrier, Complex multiblock bottle-brush architectures by RAFT polymerization, *Chem. Commun.*, 2017, **53**, 11901–11904.

13 H. G. Börner, D. Duran, K. Matyjaszewski, M. Da Silva and S. S. Sheiko, Synthesis of molecular brushes with gradient in grafting density by atom transfer polymerization, *Macromolecules*, 2002, **35**, 3387–3394.

14 X. Liang, Y. Liu, J. Huang, L. Wei and G. Wang, Synthesis and characterization of novel barbwire-like graft polymers poly(ethylene oxide)-*g*-poly(ε-caprolactone)$_4$ by the 'grafting from' strategy, *Polym. Chem.*, 2015, **6**, 466–475.

15 D. Uhrig and J. W. Mays, Synthesis of Combs, Centipedes, and Barbwires: Poly(isoprene-*graft*-styrene) Regular Multigraft Copolymers with Trifunctional, Tetrafunctional, and Hexafunctional Branch Points, *Macromolecules*, 2002, **35**(19), 7182–7190.

16 T. Pelras, C. S. Mahon, Nonappa, O. Ikkala, A. H. Gröschel and M. Müllner, Polymer Nanowires with Highly Precise Internal Morphology and Topography, *J. Am. Chem. Soc.*, 2018, **140**(40), 12736–12740.

17 B. M. Rosen, C. J. Wilson, D. A. Wilson, M. Peterca, M. R. Imam and V. Perec, Dendron-mediated self-assembly, disassembly, and self-organization of complex systems, *Chem. Rev.*, 2009, **109**, 6275–6540.

18 C. W. Evans, D. Ho, J. B. Marlow, J. J. King, C. Hee, L. N. Wong, R. Atkin, N. M. Smith, G. G. Warr, M. Norret and K. S. Iyer, Intracellular Communication between Synthetic Macromolecules, *J. Am. Chem. Soc.*, 2022, **144**(31), 14112–14120.

19 M. Kröger, O. Peleg and A. Halperin, From Dendrimers to Dendronized Polymers and Forests: Scaling Theory and its Limitations, *Macromolecules*, 2010, **43**, 6213–6224.

20 O. V. Borisov, A. A. Polotsky, O. V. Rud, E. B. Zhulina, F. A. M. Leermakers and T. M. Birshtein, Dendron Brushes and Dendronized Polymers: A Theoretical Outlook, *Soft Matter*, 2014, **10**, 2093–2101.

21 I. V. Mikhailov, A. A. Darinskii, E. B. Zhulina, O. V. Borisov and F. A. M. Leermakers, Persistence length of dendronized polymers: the self-consistent field theory, *Soft Matter*, 2015, **11**, 9367–9378.

22 C. Konak, T. Reschel, D. Oupicky and K. Ulbrich, Thermally controlled association in aqueous solutions of poly(l-lysine) grafted with poly(N-isopropylacrylamide), *Langmuir*, 2002, **18**, 8217–8222.

23 X. Jiang, G. Lu, C. Feng, Y. Li and X. Huang, Poly(acrylic acid)-*graft*-poly(N-vinylcaprolactam): A novel pH and thermo dual-stimuli responsive system, *Polym. Chem.*, 2013, **4**, 3876–3884.

24 D. Zhang, E. Dashtimoghadam, F. Fahimipour, X. Hu, Q. Li, E. A. Bersenev, D. A. Ivanov, M. Vatankhah-Varnoosfaderani and S. S. Sheiko, Tissue-adaptive materials with independently regulated modulus and transition temperature, *Adv. Mater.*, 2020, **32**, 2005314, DOI: **10.1002/adma.202005314**.

25 F. Vashahi, M. R. Martinez, E. Dashtimoghadam, F. Fahimipour, A. N. Keith, E. A. Bersenev, D. A. Ivanov, E. B. Zhulina, P. Popryadukhin, K. Matyjaszewski, M. Vatankhah-Varnosfaderani and S. S. Sheiko, Injectable bottlebrush hydrogels with tissue-mimetic mechanical properties, *Sci. Adv.*, 2022, **8**, eabm2469, DOI: **10.1126/sciadv.abm2469**.

26 M. Jacobs, H. Liang, E. Dashtimoghadam, B. J. Morgan, S. S. Sheiko and A. V. Dobrynin, Nonlinear Elasticity and Swelling of Comb and Bottlebrush Networks, *Macromolecules*, 2019, **52**, 5095–5101.

27 O. V. Borisov and E. B. Zhulina, Amphiphilic Graft Copolymers in a Selective Solvent: Intramolecular Structures and Conformational Transitions, *Macromolecules*, 2005, **38**, 2506–2514.

28 P. Kosovan, J. Kuldova, Z. Limpouchova, K. Prochazka, E. B. Zhulina and O. V. Borisov, Amphiphilic Graft Copolymers in Selective Solvents: Molecular Dynamics Simulations and Scaling Theory, *Macromolecules*, 2009, **42**, 6748–6760.

29 V. M. Prokacheva, O. V. Rud, F. Uhlik and O. V. Borisov, Intramolecular micellization and nanopatterning in pH- and thermo-responsive molecular brushes, *Soft Matter*, 2020, **16**, 208–218.

30 O. V. Borisov, O. V. Shavykin and E. B. Zhulina, Theory of polyelectrolyte dendrigrafts, *Colloid Polym. Sci.*, 2020, **298**, 951–959.

31 T. M. Birshtein, O. V. Borisov, Y. B. Zhulina, A. R. Khokhlov and T. A. Yurasova, Conformations of comb-like macromolecules, *Polym. Sci. U.S.S.R.*, 1987, **29**, 1293–1300.

32 G. H. Fredrickson, Surfactant-induced lyotropic behavior of flexible polymer solutions, *Macromolecules*, 1993, **26**, 2825–2831.

33 O. V. Borisov, T. M. Birshtein and Y. B. Zhulina, Temperature-Concentration Diagram of State for Solutions of Comb-like Macromolecules, *Polym. Sci. U.S.S.R.*, 1987, **29**, 1552–1559.

34 E. B. Zhulina, S. S. Sheiko and O. V. Borisov, Solution and Melts of Barbwire Bottlebrushes: Hierarchical Structure and Scale-Dependent Elasticity, *Macromolecules*, 2019, **52**(4), 1671–1684.

35 S. S. Sheiko, O. V. Borisov, S. A. Prokhorova and M. Möller, Cylindrical molecular brushes under poor solvent conditions: microscopic observations and scaling analysis, *Eur. Phys. J. E: Soft Matter Biol. Phys.*, 2004, **13**, 125–131.

36 A. V. Subbotin and A. N. Semenov, Spatial Self-Organization of Comb Macromolecules, *Polym. Sci., Ser. A*, 2007, **49**, 1328–1357.

37 Y. Nakamura, Intermolecular interactions of brush-like polymers, *Polym. J.*, 2011, **43**, 757–761.

38 L. Feuz, F. A. M. Leermakers, M. Textor and O. Borisov, Bending rigidity and induced persistence length of molecular bottle brushes: A self-consistent-field theory, *Macromolecules*, 2005, **38**, 8891–8901.

39 M. Saariaho, O. Ikkala, I. Szleifer, I. Erukhimovich and G. ten Brinke, On lyotropic behavior of molecular bottlebrushes: A Monte Carlo computer simulation study, *J. Chem. Phys.*, 1997, **107**, 3267–3276.

40 M. Saariaho, I. Szleifer, O. Ikkala and G. ten Brinke, Extended conformations of isolated molecular bottlebrushes: Influence of side-chain topology, *Macromol. Theory Simul.*, 1998, **7**, 211–216.

41 A. Subbotin, M. Saariaho, O. Ikkala and G. ten Brinke, Elasticity of comb copolymer cylindrical brushes, *Macromolecules*, 2000, **33**, 3447–3452.

42 S. Elli, F. Ganazzoli, E. G. Timoshenko, Y. A. Kuznetsov and R. Connolly, Size and persistence length of molecular bottle-brushes by Monte Carlo simulations, *J. Chem. Phys.*, 2004, **120**, 6257–6267.

43 P. E. Theodorakis, H.-P. Hsu, W. Paul and K. Binder, Computer simulation of bottle-brush polymers with flexible backbone: Good solvent versus theta solvent conditions, *J. Chem. Phys.*, 2011, **135**, 164903.

44 Z. Cao, J.-M. Y. Carrillo, S. S. Sheiko and A. V. Dobrynin, Computer Simulations of Bottle Brushes: From Melts to Soft Networks, *Macromolecules*, 2015, **48**, 5006–5015.

45 M. Jacobs, H. Liang, B. Pugnet and A. V. Dobrynin, Molecular Dynamics Simulations of Surface and Interfacial Tension of Graft Polymer Melts, *Langmuir*, 2018, **34**(43), 12974–12981.

46 H.-P. Hsu, W. Paul and K. Binder, Standard definitions of persistence length do not describe the local intrinsic stiffness of real polymer chains, *Macromolecules*, 2010, **43**, 3094–3102.

47 H.-P. Hsu, W. Paul and K. Binder, Estimation of persistence lengths of semiflexible polymers: Insight from simulations, *Polym. Sci., Ser. C*, 2013, **55**, 39–59.

48 E. Muhammadi, S. J. Joshi and S. A. Deshmukh, Review of computational studies of bottlebrush polymers, *Comput. Mater. Sci.*, 2021, **199**, 110720.

49 S. S. Sheiko and A. V. Dobrynin, Architectural Code for Rubber Elasticity: from Supersoft to Superfirm Materials, *Macromolecules*, 2019, **52**, 7531–7546.

50 J. Rzayev, Synthesis of polystyrene-polylactide bottlebrush block copolymers and their melt self-assembly into large domain nanostructures, *Macromolecules*, 2009, **42**, 2135–2141.

51 A. L. Liberman-Martin, C. K. Chu and R. H. Grubbs, Application of Bottlebrush Block Copolymers as Photonic Crystals, *Macromol. Rapid Commun.*, 2017, **38**, 1700058.

52 M. Vatankhah-Varnosfaderani, A. N. Keith, Y. Cong, H. Liang, M. Rosenthal, M. Sztucki, C. Clair, S. Magonov, D. A. Ivanov, A. V. Dobrynin and S. S. Sheiko, Chameleon-like elastomers with molecularly encoded strain-adaptive stiffening and coloration, *Science*, 2018, **359**(6383), 1509–1513.

53 D. P. Song, T. H. Zhao, G. Guidetti, S. Vignolini and R. M. Parker, Hierarchical Photonic Pigments via the Confined Self-Assembly of Bottlebrush Block Copolymers, *ACS Nano*, 2019, **13**, 1764–1771.

54 L. Leibler, Theory of Microphase Separation in Block Copolymers, *Macromolecules*, 1980, **13**(6), 1602–1617.

55 A. N. Semenov, Contribution to the Theory of Microphase Layering in Block-Copolymer Melts, *Sov. Phys. – JETP*, 1985, **61**, 733–742.

56 M. W. Matsen and F. S. Bates, Unifying Weak- and Strong-Segregation Block Copolymer Theories, *Macromolecules*, 1996, **29**(4), 1091–1098.

57 C. M. Bates and F. S. Bates, 50th Anniversary Perspective: Block Polymers Pure Potential, *Macromolecules*, 2017, **50**, 3–22.

58 J. V. Liu, C. J. García-Cervera, K. T. Delaney and G. H. Fredrickson, Optimized Phase Field Model for Diblock Copolymer Melts, *Macromolecules*, 2019, **52**, 2878–2888.

59 V. V. Vasilevskaya, L. A. Gusev, A. R. Khokhlov, O. Ikkala and G. ten Brinke, Domains in Melts of Comb-Coil Diblock Copolymers: Superstrong Segregation Regime, *Macromolecules*, 2001, **34**, 5019–5022.

60 S. J. Dalsin, T. G. Rions-Maehren, M. D. Beam, F. S. Bates, M. A. Hillmyer and M. W. Matsen, Bottlebrush Block Polymers: Quantitative Theory and Experiments, *ACS Nano*, 2015, **9**(12), 12233–12245.

61 R. K. W. Spencer and M. W. Matsen, Field-theoretic simulations of bottlebrush copolymers, *J. Chem. Phys.*, 2018, **149**, 184901.

62 A. E. Levi, J. Lequieu, J. D. Horne, M. W. Bates, J. M. Ren, K. T. Delaney, G. H. Fredrickson and C. M. Bate, Miktoarm Stars via Grafting-Through Copolymerization: Self-Assembly and the Star-to-Bottlebrush Transition, *Macromolecules*, 2019, **52**(4), 1794–1802.

63 E. B. Zhulina, S. S. Sheiko and O. V. Borisov, Theory of microphase segregation in the melts of copolymers with dendritically branched, bottlebrush or cycled blocks, *ACS Macro Lett.*, 2019, **8**, 1075–1079.

64 E. B. Zhulina, S. S. Sheiko, A. V. Dobrynin and O. V. Borisov, Microphase segregation in the melts of bottlebrush block copolymers, *Macromolecules*, 2020, **53**(7), 2582–2593.

65 I. V. Mikhailov, E. B. Zhulina and O. V. Borisov, Brushes and lamellar mesophases of comb-shaped (co)polymers: a self-consistent field theory, *Phys. Chem. Chem. Phys.*, 2020, **22**, 23385–23398.

66 I. V. Mikhailov, F. A. M. Leermakers, A. A. Darinskii, E. B. Zhulina and O. V. Borisov, Theory of microphase segregation in ABA triblock comb-shaped copolymers: lamellar mesophase, *Macromolecules*, 2021, **54**, 4747–4759.
67 E. B. Zhulina, I. V. Mikhailov and O. V. Borisov, Theory of mesophases of triblock comb-shaped copolymers. Effects of dead zones and bridging, *Macromolecules*, 2022, **55**(14), 6040–6055.
68 S. J. Park, G. K. Cheong, F. S. Bates and K. D. Dorfman, Stability of the Double Gyroid Phase in Bottlebrush Diblock Copolymer Melts, *Macromolecules*, 2021, **54**, 9063–9070.
69 J. Zhang, D. K. Schneiderman, T. Li, M. A. Hillmyer and F. S. Bates, Design of Graft Block Polymer Thermoplastics, *Macromolecules*, 2016, **49**(23), 9108–9118.
70 J. Bolton, T. S. Baile and J. Rzayev, Large pore size nanoporous materials from self-assembly of asymmetric bottlebrush block copolymers, *Nano Lett.*, 2011, **11**, 998–1001.
71 Y. Gai, D.-P. Song, B. M. Yavitt and J. J. Watkins, Polystyrene-*block*-poly(ethylene oxide) Bottlebrush Block Copolymer Morphology Transitions: Influence of Side Chain Length and Volume Fraction, *Macromolecules*, 2017, **50**, 1503–1511.
72 M. B. Runge and N. B. Bowden, Synthesis of High Molecular Weight Comb Block Copolymers and Their Assembly into Ordered Morphologies in the Solid State, *J. Am. Chem. Soc.*, 2007, **129**, 10551–10560.
73 M. B. Runge, C. E. Lipscomb, L. R. Ditzler, M. K. Mahanthappa, A. V. Tivanski and N. B. Bowden, Investigation of the Assembly of Comb Block Copolymers in the Solid State, *Macromolecules*, 2008, **41**, 7687–7694.
74 H.-F. Fei, B. M. Yavitt, X. Hu, G. Kopanati, A. Ribbe and J. J. Watkins, Influence of Molecular Architecture and Chain Flexibility on the Phase Map of Polystyrene-*block*-poly(dimethylsiloxane) Brush Block Copolymers, *Macromolecules*, 2019, **52**, 6449–6457.
75 D. F. Sunday, A. B. Chang, C. D. Liman, E. Gann, D. M. Delongchamp, L. Thomsen, M. W. Matsen, R. H. Grubbs and C. L. Soles, Self-Assembly of ABC Bottlebrush Triblock Terpolymers with Evidence for Looped Backbone Conformations, *Macromolecules*, 2019, **52**(4), 1557–1566.
76 J. Bolton and J. Rzayev, Synthesis and Melt Self-Assembly of PS-PMMA-PLA Triblock Bottlebrush Copolymers, *Macromolecules*, 2014, **47**, 2864–2874.
77 S. Nian, H. Lian, Z. Gong, M. Zhernenkov, J. Qin and L.-H. Cai, Molecular Architecture Directs Linear-Bottlebrush-Linear Triblock Copolymers to Self-Assemble to Soft Reprocessable Elastomers, *ACS Macro Lett.*, 2019, **8**, 1528–1534.
78 M. Zamurovic, S. Christodoulou, A. Vazaios, E. Iatrou, M. Pitsikalis and N. Hadjichristidis, Micellization Behavior of Complex Comblike Block Copolymer Architectures, *Macromolecules*, 2007, **40**, 5835–5849.
79 Z. Li, J. Ma, C. Xheng, K. Zhang and K. L. Wooley, Synthesis of Hetero-Grafted Amphiphilic Diblock Molecular Brushes and Their Self-Assembly in Aqueous Medium, *Macromolecules*, 2010, **43**, 1182–1184.
80 R. Fenyves, M. Schmutz, I. J. Horner, F. V. Bright and J. Rzayev, Aqueous Self-Assembly of Giant Bottlebrush Block Copolymer Surfactants as Shape-Tunable Building Blocks, *J. Am. Chem. Soc.*, 2014, **136**, 7762–7770.
81 M. Alaboalirat, L. Qi, K. J. Arrington, S. Qian, J. K. Keum, H. Mei, K. C. Littrell, B. G. Sumpter, J.-M. Y. Carrillo, R. Verduzco and J. B. Matson, Amphiphilic Bottlebrush Block copolymers: Analysis of Aqueous Self-Assembly by Small-Angle Neutron Scattering and Surface Tension Measurements, *Macromolecules*, 2019, **52**(2), 465–476.
82 S. Kim, Y. Cho, J. H. Kim, S. Song, J. Lim, S.-H. Choi and K. Char, Structural Analysis of Bottlebrush Block Copolymer Micelles Using Small-angle X-ray Scattering, *ACS Macro Lett.*, 2020, **9**, 1261–1266.
83 E. Taipaleenmaki, S. A. Mouritzen, P. Schattling, Y. Zhang and B. Städler, Mucopenetrating micelles with a PEG corona, *Nanoscale*, 2017, **9**(46), 18438–18448.
84 Y. Wang, F. Shao, E. R. Sauve, C. M. Tonge and Z. M. Hudson, Self-assembly of giant bottlebrush block copolymer surfactants from luminescent organic electronic materials, *Soft Matter*, 2019, **15**, 5421–5430.
85 H. Unsal, S. Onbulak, F. Calik, M. Er-Rafik, M. Schmutz, A. Sanyal and J. Rzayev, Interplay between Molecular Packing, Drug Loading, and Core Cross-Linking in Bottlebrush Copolymer Micelles, *Macromolecules*, 2017, **50**(4), 1342–1352.
86 B. B. Patel, T. Pan, Y. Chang, D. J. Walsh, J. J. Kwok, K. S. Park, K. Patel, D. Guironnet, C. E. Sing and Y. Diao, Concentration-Driven Self-Assembly of PS-*b*-PLA Bottlebrush Diblock Copolymers in Solution, *ACS Polym. Au*, 2022, **2**, 232–244.
87 M. Alaboalirat, L. Qi, K. J. Arrington, S. Qian, J. K. Keum, H. Mei, K. C. Littrell, B. G. Sumpter, J.-M. Y. Carrillo, R. Verduzco and J. B. Matson, Amphiphilic Bottlebrush Block Copolymers: Analysis of Aqueous Self-Assembly by Small-Angle Neutron Scattering and Surface Tension Measurements, *Macromolecules*, 2019, **52**(2), 465–476.
88 Y. Shibuya, H. V.-T. Nguyen and J. A. Johnson, Mikto-Brush-Arm Star Polymers via Cross-Linking of Dissimilar Bottlebrushes: Synthesis and Solution Morphologies, *ACS Macro Lett.*, 2017, **6**(9), 963–968.
89 D. M. Henn, J. A. Holmes, E. W. Kent and B. Zhao, Worm-to-Sphere Shape Transition of Thermoresponsive Linear Molecular Bottlebrushes in Moderately Concentrated Aqueous Solution, *J. Phys. Chem. B*, 2018, **122**(27), 7015–7025.
90 E. B. Zhulina and O. V. Borisov, Micelles Formed by AB Copolymer with Bottlebrush blocks. Scaling Theory, *J. Phys. Chem. B*, 2021, **125**(45), 12603–12616.
91 I. O. Lebedeva, E. B. Zhulina and O. V. Borisov, Self-assembly of bottlebrush block copolymers in selective solvent: micellar structures, *Polymers*, 2021, **13**, 1351–1365.
92 T. Li, F. Huang, D. Diaz-Dussan, J. Zhao, S. Srinivas, R. Narain, W. Tian and X. Hao, Preparation and Characterization of Thermoresponsive PEG-Based Injectable Hydrogels and Their Application for 3D Cell Culture, *Biomacromolecules*, 2020, **21**, 1254–1263.

93 J. M. Sarapas, E. P. Chan, E. M. Rettner and K. L. Beers, Compressing and Swelling To Study the Structure of Extremely Soft Bottlebrush Networks Prepared by ROMP, *Macromolecules*, 2018, **51**(6), 2359–2366.

94 S. S. Sheiko, F. Vashahi, B. J. Morgan, M. Maw, E. Dashtimoghadam, F. Fahimipour, M. Jacobs, A. N. Keith, M. Vatankhah-Varnosfaderani and A. V. Dobrynin, Mechanically Diverse Gels with Equal Solvent Content, *ACS Cent. Sci.*, 2022, **8**(6), 845–852.

95 E. B. Zhulina, S. S. Sheiko and O. V. Borisov, Polymer Networks Formed by Molecular Brushes: Scaling Theory, *Polym. Sci., Ser. A*, 2019, **61**(6), 799–804.

96 E. B. Zhulina and O. V. Borisov, Bottlebrush polymer gels: architectural control over swelling and elastic moduli, *Soft Matter*, 2022, **18**, 1239–1246.

97 H. Liang, Z. Cao, Z. Wang, S. S. Sheiko and A. V. Dobrynin, Combs and Bottlebrushes in a Melt, *Macromolecules*, 2017, **50**(8), 3430–3437.

98 H. Liang, B. J. Morgan, G. Xie, M. R. Martinez, E. B. Zhulina, K. Matyjaszewski, S. S. Sheiko and A. V. Dobrynin, Universality of the Entanglement Plateau Modulus of Comb and Bottlebrush Polymer Melts, *Macromolecules*, 2018, **51**(23), 10028–10039.

99 J. J. Paturej, S. S. Sheiko, S. Panyukov and M. Rubinstein, Molecular Structure of Bottlebrush Polymers in Melts, *Sci. Adv.*, 2016, **2**, e1601478.

100 Ye. B. Zhulina and T. M. Birshtein, Composition-concentration diagram of superstructures of diblock copolymers, *Polym. Sci. U.S.S.R.*, 1987, **29**(7), 1678–1685.

101 M. Daoud and J.-P. Cotton, Star shaped polymers, *J. Phys.*, 1982, **43**, 531–538.

102 P.-G. de Gennes, *Scaling Concepts in Polymer Physics*, Cornell University Press, Ithaca and London, 1979.

103 S. Dutta, T. Pan and C. E. Sing, Bridging Simulation Length Scales of Bottlebrush Polymers Using a Wormlike Cylinder Model, *Macromolecules*, 2019, **52**(13), 4858–4874.

104 S. Dutta and C. E. Sing, Two Stretching Regimes in the Elasticity of Bottlebrush Polymers, *Macromolecules*, 2020, **53**(16), 6946–6955.

105 J.-F. Gohy, Block Copolymer Micelles, *Adv. Polym. Sci.*, 2005, **190**(1), 65–136.

106 M. Lazzari, G. Lin and S. Lecommandoux, *Block copolymers in nanoscience*, Wiley-VCH, Weinheim, 2006.

107 O. V. Borisov, E. B. Zhulina, F. A. M. Leermakers and A. H. E. Müller, Self-Assembled Structures of Amphiphilic Ionic Block Copolymers: Theory, Self-Consistent Field Modeling and Experiment, *Adv. Polym. Sci.*, 2011, **241**, 57–130.

108 K. Kataoka, A. Harada and Y. Nagasaki, Block copolymer micelles for drug delivery: design, characterization and biological significance, *Adv. Drug Delivery Rev.*, 2001, **47**(1), 113–131.

109 V. Ibrahimova, H. Zhao, E. Ibarboure, E. Garanger and S. Lecommandoux, Thermosensitive vesicles from chemically encoded lipid-grafted elastin-like polypeptides, *Angew. Chem., Int. Ed.*, 2021, **60**, 15036–15040.

110 S. Alexander, Adsorption of chain molecules with a polar head: a scaling description, *J. Phys.*, 1977, **38**, 983–987.

111 P.-G. de Gennes, Conformations of Polymers Attached to an Interface, *Macromolecules*, 1980, **13**, 1069–1075.

112 P.-G. De Gennes, Macromolecules and Liquid Crystals: Reflections on Certain Lines of Research, *Solid State Phys.*, 1978, **14**(Suppl.), 1–18.

113 Ye. B. Zhulina and T. M. Birshtein, Conformations of Block Copolymer Molecules in Selective Solvents. (Micellar Structures), *Polym. Sci. U.S.S.R.*, 1985, **27**, 570–578.

114 T. M. Birshtein and E. B. Zhulina, Scaling Theory of Supermolecular Structures in Block Copolymer – Solvent Systems. 1. Model of Micellar Structures, *Polymer*, 1989, **30**(1), 170–177.

115 A. Halperin, Polymeric micelles: a star model, *Macromolecules*, 1987, **20**(11), 2943–2946.

116 L. A. Volkova, N. A. Andreeva, A. F. Podolosky, M. I. Bitsenko and V. A. Eskin, Study of mesomorphic properties of solutions of triblock copolymer: polyisoprene-poly-α-methyl styrene-polyisoprene, *Vysokomol. Soedin. A*, 1982, **24**, 1180–1185.

117 M. Shibayama, T. Hashimoto and H. Kawai, Ordered structure in block polymer solutions. 1. Selective solvents, *Macromolecules*, 1983, **16**, 16–28.

118 J. J. Molina, C. Pierleoni, B. Capone, J.-P. Hansen and I. S. Santos de Oliveira, Crystal stability of Diblock Copolymer Micelles in Solution, *Mol. Phys.*, 2009, **107**(4–6), 535–548.

119 E. B. Zhulina, M. Adam, S. Sheiko, I. LaRue and M. Rubinstein, Diblock Copolymer Micelles in a Dilute Solution, *Macromolecules*, 2005, **38**(12), 5330–5351.

120 A. E. Marras, T. R. Campagna, J. R. Vieregg and M. V. Tirrell, Physical Property Scaling Relationships for Polyelectrolyte Complex Micelles, *Macromolecules*, 2021, **54**(13), 6585–6594.

121 I. Larue, M. Adam, E. B. Zhulina, M. Rubinstein, M. Pitsikalis, N. Hadjichristidis, D. A. Ivanov, R. I. Gearba, D. V. Anokhin and S. S. Sheiko, Effect of the Soluble Block Size on Spherical Diblock Copolymer Micelles, *Macromolecules*, 2008, **41**(17), 6555–6563.

122 G. T. Pickett, Classical Path Analysis of end-Grafted Dendrimers: Dendrimer Forest, *Macromolecules*, 2001, **34**, 8784–8791.

123 T. C. Zook and G. T. Pickett, Hollow-Core Dendrimers Revised, *Phys. Rev. Lett.*, 2003, **90**(1), 015502.

124 A. A. Polotsky, F. A. M. Leermakers, E. B. Zhulina and T. M. Birshtein, On the Two-Population Structure of Brushes Made of Arm-Grafted Polymer Stars, *Macromolecules*, 2012, **45**, 7260–7273.

125 E. B. Zhulina, F. A. M. Leermakers and O. V. Borisov, Ideal mixing in multicomponent brushes of branched macromolecules, *Macromolecules*, 2015, **48**(23), 5614–5622.

126 E. B. Zhulina, F. A. M. Leermakers and O. V. Borisov, Brushes of Cycled Macromolecules: Structure and Lubricating Properties, *Macromolecules*, 2016, **49**(22), 8758–8767.

127 A. M. Skvortsov, L. I. Klushin and A. A. Gorbunov, Long and short chains in a polymer brush: a conformational transition, *Macromolecules*, 1997, **30**(6), 1818–1827.

128 G. M. Leuty, M. Tsige, G. S. Grest and M. Rubinstein, Tension amplification in tethered layers of bottle-brush polymers, *Macromolecules*, 2016, **49**(5), 1950–1960.
129 G. J. Fleer, M. A. Cohen Stuart, J. M. H. M. Scheutjens, T. Cosgrove and B. Vincent, *Polymers at Interfaces*, Chapman and Hall, London, 1993.
130 H. Liang, Z. Wang and A. V. Dobrynin, Strain-Adaptive Self-Assembled Networks of Linear-Bottlebrush-Linear Copolymers, *Macromolecules*, 2019, **52**, 8617–8624.
131 Z. Cao, W. F. M. Daniel, M. Vatankhah-Varnosfaderani, S. S. Sheiko and A. V. Dobrynin, Dynamics of Bottlebrush Networks, *Macromolecules*, 2016, **49**(20), 8009–8017.
132 O. V. Borisov and E. B. Zhulina, Conformations of polyelectrolyte molecular brushes: a meanfield theory, *J. Chem. Phys.*, 2018, **149**, 184904.
133 C. Kiani, L. Chen, Y. J. Wu, A. J. Yee and B. B. Yang, Structure and functions of aggrecan, *Cell Res.*, 2002, **12**, 19–32.
134 X. Liu and P. M. Claesson, Bioinspired Bottlebrush Polymers for Aqueous Boundary Lubrication, *Polymers*, 2022, **14**, 2724.
135 X. Liu, A. Dedinaite, M. Rutland, E. Thormann, C. Visnevskij, R. Makuska and P. M. Claesson, Electrostatically Anchored Branched Brush Layers, *Langmuir*, 2012, **28**, 15537–15547.
136 X. Banquy, J. Burdinska, D. W. Lee, K. Matyjaszewski and J. Israelachvili, Bioinspired Bottle-Brush Polymer Exhibits Low Friction and Amontons-like Behavior, *J. Am. Chem. Soc.*, 2014, **136**, 6199–6202.
137 O. V. Borisov, E. B. Zhulina, A. A. Polotsky, F. A. M. Leermakers and T. M. Birshtein, Interactions between brushes of root-tethered dendrons, *Macromolecules*, 2014, **47**(19), 6932–6945.